DSP ALGORITHM AND SYSTEM DESIGN FOR UWB COMMUNICATION SYSTEMS

YANG LIU

(B.Eng.(Hons.), NTU)

A THESIS SUBMITTED

FOR THE DEGREE OF MASTER OF ENGINEERING

DEPARTMENT OF ELECTRICAL & COMPUTER ENGINEERING

NATIONAL UNIVERSITY OF SINGAPORE

2006

ACKNOWLEDGEMENT

I would like to express my utmost appreciation to my supervisors, Dr. Zheng Yuanjin and Prof. Hari Krishna Garg, for being so understanding, helpful and encouraging at all times through my research and study in National University of Singapore and Institute of Microelectronics. I am especially grateful for the invaluable guidance and constructive suggestions offered by Dr. Zheng throughout the development of this dissertation.

I would also like to thank my friends, Mr. Cao Mingzheng, Miss Yan Jiangnan, Mr. Cao Rui, Mr. Tong Yan, Miss Zhou Qiaoer, Miss Wei Xiaoqian and Miss Lu Miaomiao, for their kindness and supportive work.

Many thanks to my family, for always being there for me, whenever and wherever.

Lastly I also wish to extend my appreciation to all the others who have, in one way or another, helped in making this dissertation a very rewarding one.

It has been a pleasure working together.

TABLE OF CONTENTS

SUMMARY

Ultra-Wideband (UWB) communication is recognized as one of the most promising technologies for next generation Wireless Personal Area Network (WPAN) since it has the potential to provide a low complexity, low cost, low power consumption, and high data rate connectivity in communication systems. It relies on transmission of ultra-short (in nanosecond scale) pulses and avoids using sinusoidal carriers or intermediate frequency (IF) processing. One of the most significant features of UWB communication is its fine multipath resolvability. To maximally exploit the channel diversity, a Rake receiver is usually employed to effectively capture the multipath energy. Conventional Rake receivers require channel information, including the multipath delay and attenuation, to be provided before combing the multipath energy. However the channel information is unknown to the receiver and difficult to estimate in practical UWB transmission systems.

In this thesis, a novel blind Rake (BRake) structure is proposed for high data rate low power consumption UWB communication systems. The word “blind” here does not imply that training sequence can be totally eliminated, but refers to the fact that the channel information is not needed for the Rake system to perform effectively. In other words, it avoids the estimation of multipath channel which must be provided for conventional Rake receiver systems. The transceiver complexity is further reduced by using Analog-to-Digital Converter (ADC) working at sub-Nyquist sampling rate. The closed form bit error rate (BER) performance analysis is provided as well. Extensive simulations have been carried out which verified the theoretical analysis.

LIST OF FIGURES

LIST OF ABBREVIATIONS

A-STAR	Agency of Science, Technology and Research
ADC	Analog-to-Digital Converter
ARake	All Rake
ASIC	Application-Specific Integrated Circuit
AWGN	Additive White Gaussian Noise
BER	Bit Error Rate
BPSK	Binary Phase Shift Keying
BRake	Blind Rake
CFJ	Carrier Frequency Jitter
CFO	Carrier Frequency Offset
CIR	Channel Impulse Response
CM	Channel Model
CSI	Channel State Information
DC	Direct Current
DS	Direct Sequence
EIRP	Effective Isotropic Radiated Power
EM	Electromagnetic
FAS	Federal Aviation System
FCC	Federal Communication Commission
FPGA	Field Programmable Gate Array
FTT	Fast Fourier Transform

GPS	Global Positioning System
IF	Intermediate Frequency
IFTT	Inverse Fast Fourier Transform
IME	Institute of Microelectronics
IR	Impulse Radio
ISI	Inter Symbol Interference
LMS	Least Mean Square
LPD	Low Probability of Detection
LPI	Low Probability of Interception
MA	Multi-user Access
MB-OFDM	Multi-Band Orthogonal Frequency Division Multiplexing
MB-UWB	Multi-Band Ultra-Wideband
MBOA	Multi-Band OFDM Alliance
MF	Matched Filter
MFEP	Matched Front-End Processor
MMSE	Minimum Mean Square Error
MRC	Maximum Ratio Combing
MSE	Mean Square Error
NB	Narrowband
OFDM	Orthogonal Frequency Division Multiplexing
PAM	Pulse Amplitude Modulation
PDP	Power Delay Profile
PPM	Pulse Position Modulation
PRake	Partial Rake

PRT	Pulse Repetition Time
PSD	Power Spectral Density
R&O	Report & Order
RF	Radio Frequency
RMS	Root Mean Square
S-V	Saleh-Valenzuela
SNR	Signal to Noise Ratio
SRake	Selective Rake
TDL	Tapped Delay Line
TFC	Time Frequency Code
TFK	Time Frequency Kernel
U-NII	Unlicensed National Information Infrastructure
UWB	Ultra-Wideband
WLAN	Wireless Local Area Network
WPAN	Wireless Personal Area Network

LIST OF SYMBOLS

A	A factor to normalize the pulse energy
C	Channel Capacity
J	MMSE cost function
K	Total tap number in a branch
L	Total branch number
M	Total number of multipath in a channel
$\mathcal{M}$	Misadjustment
X	Channel log-normal shadowing coefficient
m	The m^{th} multipath component in a channel
W	Channel Bandwidth
$g(t)$	2^{nd} order Gaussian derivative waveform
$\mathbf{g_m}$	Gaussian pulse vector based on real channel timing
$\mathbf{g_{l,k}}$	Gaussian pulse vector based on receiver sampling timing
$h(t)$	Channel impulse response
$r(t)$	Received signal
$r_n(t)$	Received signal for n^{th} symbol
$s(t)$	Transmitted signal
$\mathbf{s_I}$	Vector of signal after correlation
$w(t)$	Noise signal

$w_{l,k}$	Noise for k^{th} tap of l^{th} branch after correlation operation
$\mathbf{w_I}$	Vector of noise mixed with signal after correlation
$\mathbf{w_{LK-I}}$	Vector of pure noise after correlation
$p_n(t)$	n^{th} order Gaussian derivative waveform in time domain
$P_n(f)$	n^{th} order Gaussian derivative waveform in frequency domain
b_n	Constellation for PAM/Transmitted symbol
$\hat{b}_n$	Estimated symbol
$\mathbf{b_n}$	Vector of training sequence
c_n^{TH}	User-specific TH code for n^{th} impulse
$c_{l,k}$	Weight for k^{th} tap of l^{th} branch
$c_n^{l,k}$	Weight for k^{th} tap of l^{th} branch for symbol n during training phase
$\mathbf{c}$	Tap weight vector
$\mathbf{c_o}$	Optimum tap weight vector
c_i^o	i^{th} optimum tap weight
c_i^{LMS}	i^{th} LMS tap weight
d_n	Constellation for PPM
e_n	Error signal for n^{th} symbol duration training phase
e_i^{LMS}	i^{th} LMS error
$v_{l,k}$	Input of the k^{th} tap in the l^{th} branch
$v_n^{l,k}$	Input of the k^{th} tap in the l^{th} branch for symbol n

$\mathbf{v}$	Tap input vector
y_n	Decision signal for n^{th} symbol
E_b	Bit energy
E_p	Pulse energy
$\mathbf{I_{P\times P}}$	$P\times P$ identity matrix
L	Number of fingers in a Rake
L_b	Number of fingers in a SRake
L_p	Number of fingers in a PRake
N_c	Number of chips in each frame
N_f	Number of replicas in each transmitted symbol
N_0	One side power spectrum density of AWGN
P_b	Bit error rate (BER)
$\mathbf{Q}$	Eigenvector matrix
$\mathbf{R}$	Tap input autocorrelation matrix
$R_g(.)$	Pulse correlation function
$S_{\tilde{h}}(\tau)$	Delay spectrum
T_c	Chip duration
T_d	Maximum excess delay of the channel
T_p	Impulse duration
T_{pr}	Pulse repetition time
T_s	Symbol duration

T_l	Channel time delay of the l^{th} cluster
σ	Standard deviation of a Gaussian random variable
$\sigma_{e_i}^2$	Variance of LMS error
$\sigma_{w_{l,k}}^2$	Variance of noise after correlation
γ	SNR ratio
ϕ	Processing gain
μ	Adaptation step size during training phase
Δ	Pulse position offset in PPM
α_m	Channel attenuation of the m^{th} multipath component
$\alpha_{k,l}$	Channel attenuation of the k^{th} multipath in the l^{th} cluster
$\boldsymbol{\alpha}_{\mathbf{m}}$	Vector of channel attenuation
τ_m	Channel delay of the m^{th} multipath component
$\tau_{k,l}$	Channel delay of the k^{th} multipath in the l^{th} cluster
$\bar{\tau}_l$	Receiver sampling interval of l^{th} branch
$\bar{\tau}_{l,k}$	Receiver sampling time of the k^{th} tap in the l^{th} branch
$\boldsymbol{\tau}_{\mathbf{m}}$	Vector of Channel delay
$\boldsymbol{\tau}_{\mathbf{lk}}$	Vector of receiver sampling time
τ_{RMS}	Channel RMS delay spread
$\Delta\tau$	Delay between consecutive BRake branch
Λ	Cluster arrival rate of channel multipath
$\boldsymbol{\Lambda}_{\mathbf{S}}$	Diagonal eigenvalue matrix

ς_i	i^{th} Eigenvalue
λ	Ray arrival rate of channel multipath in a cluster
λ_i	i^{th} eigenvalue of autocorrelation matrix of input data
η	Successfully collected channel energy
$E[\cdot]$	Expectation operation
$\delta(\cdot)$	Dirac delta function
$Q(\cdot)$	Complementary cumulative distribution function
$tr(\cdot)$	Matrix trace operation
$\otimes$	Convolution operation

1 INTRODUCTION

This chapter gives a brief introduction of UWB communication systems. UWB technology has been in used for more than a century. However it attracts real attention both in industry and academy only after the Federal Communication Commission (FCC) released a huge “new bandwidth” of 3.1-10.6 GHz for it in 2002. UWB applications include, but not limit to, Wireless Personal Area Networks (WPANs), sensor networks, imaging systems, vehicular radar systems, etc.

The scope and organization of the whole thesis are also presented in this chapter.

1.1 Background

Scientists and engineers have known about UWB signals since Guglielmo Marconi invented radio communications utilizing enormous bandwidth as information was conveyed by spark-gap devices more than a century ago. However the signals were more difficult to control or detect than narrowband (NB, single-frequency) signals at that time. Modern UWB technology came into the picture since 1960s, when the introduction of UWB impulse radar systems was motivated by the high sensitivity to scatters and low power consumption applications [1]-[3]. Commercially, the early UWB investigation was largely under the aegis of the U. S. Department of Defense that adopted wideband signals primarily for very accurate localization and imaging in the context of secure communications [4], [5]. Academically, the UWB research and development were largely pioneered by Prof. Scholtz and his group [6]-[9], [13], [28], [29], [32], focusing mainly on low-rate applications.

UWB, as the name suggests, occupies a very large bandwidth for signal transmission while the emission power is well below conventional narrowband or wideband systems. Figure 1.1 below illustrates this concept. UWB pulses spread energy over several-gigahertz range of frequencies, as opposed to traditional narrowband, which covers a limited band of about 30 kilohertz. Cellular phones operate in the wideband, which covers about 5 megahertz.

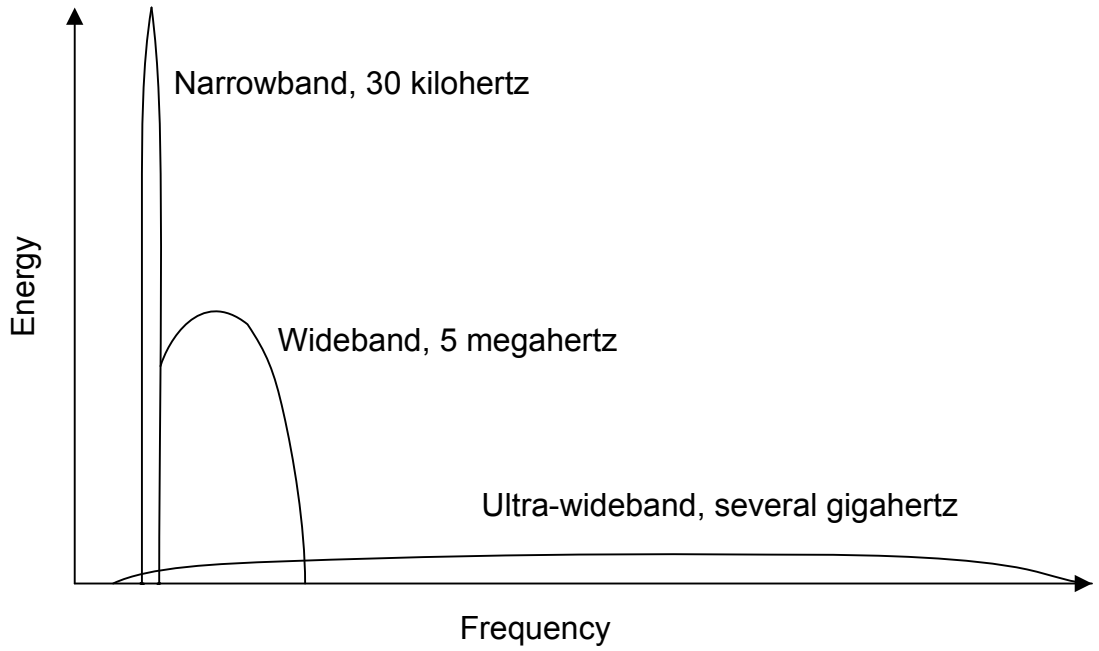

Figure 1.1 Frequency & energy comparison for communication systems.

The definition of UWB evolves with time. The rule making of UWB was opened by FCC in 1998. The resulting First Report and Order (R&O) that permitted deployment of UWB devices was announced on 14 February and released in April 2002 [10], which unleashed a very large bandwidth of 3.1-10.6 GHz to UWB transmissions. Three types of UWB systems are defined in this R&O: imaging systems, communication and measurement systems, and vehicular radar systems. Specifically, UWB characterizes transmission systems with instantaneous spectral occupation in excess of 500 MHz or a fractional bandwidth of more than 20%.

The bandwidth and spectral mask for indoor communication systems assigned by FCC is illustrated in Figure 1.2. It can be seen that the FCC regulated power levels are very low (below -41.3 dBm), which allows UWB technology to coexist with legacy services such as IEEE 802.11a wireless local area network (WLAN), radar systems, etc., as well as

overlay with sensitive military and civilian services in adjacent bands such as global positioning system (GPS) and federal aviation system (FAS). Cellular phones, for example, transmit up to +30 dBm, which is equivalent to 10^7 higher power spectral density (PSD) than UWB transmitters are permitted [11]. Currently the IEEE 802.15 Working Group is putting efforts to standardize UWB wireless radios for indoor multimedia transmissions.

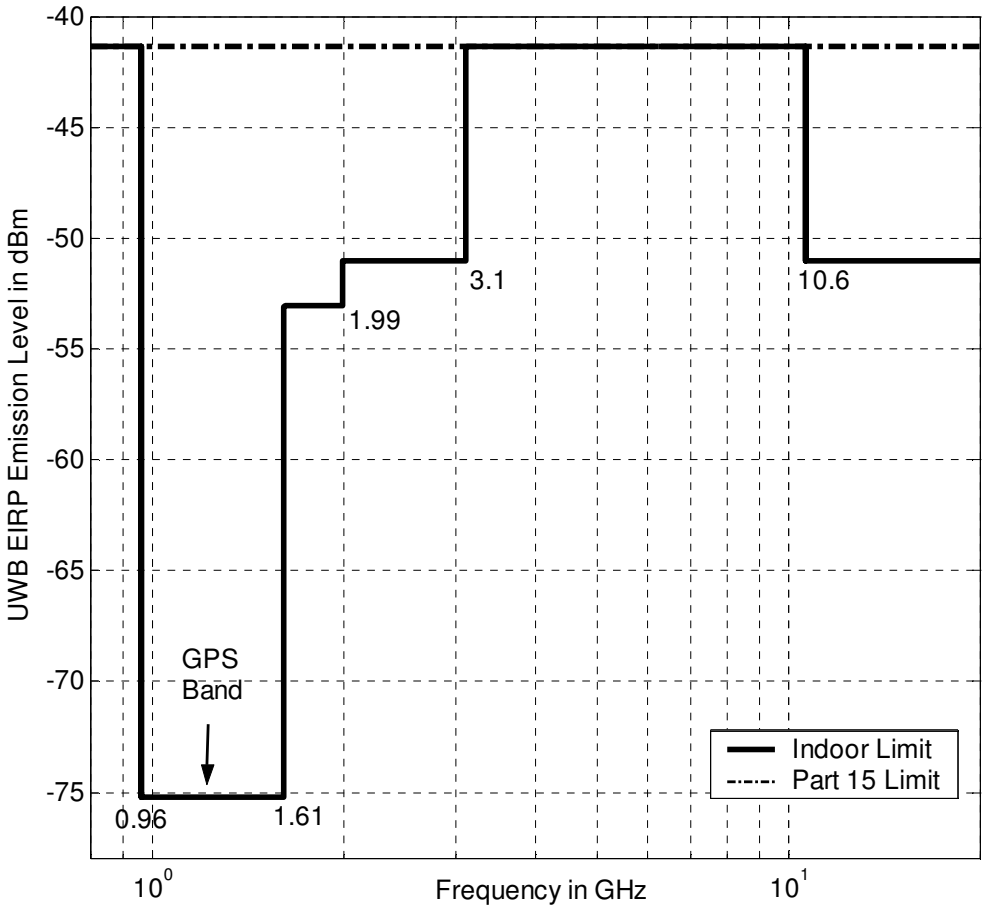

Figure 1.2 FCC regulated spectral mask for UWB indoor communication systems.

Based on the FCC regulation, UWB is mostly suitable for the short-range high-speed

applications among other wireless systems, as can be seen in Figure 1.3. From Shannon's theory [12],

$$C = 1.44 \times W \times \log_2(1 + SNR), \tag{1.1}$$

where C standards for the channel capacity in bits per second, W represents the channel bandwidth in hertz and SNR is the signal to noise ratio, the channel transmission rate grows *linearly* with channel bandwidth but only *logarithmically* with SNR. In other words, the channel capacity increases much faster as a function of bandwidth than power. Thus UWB has the potential to offer high data rate (in several hundred megabit per second, Mbps) to emerging high-speed-demanding applications.

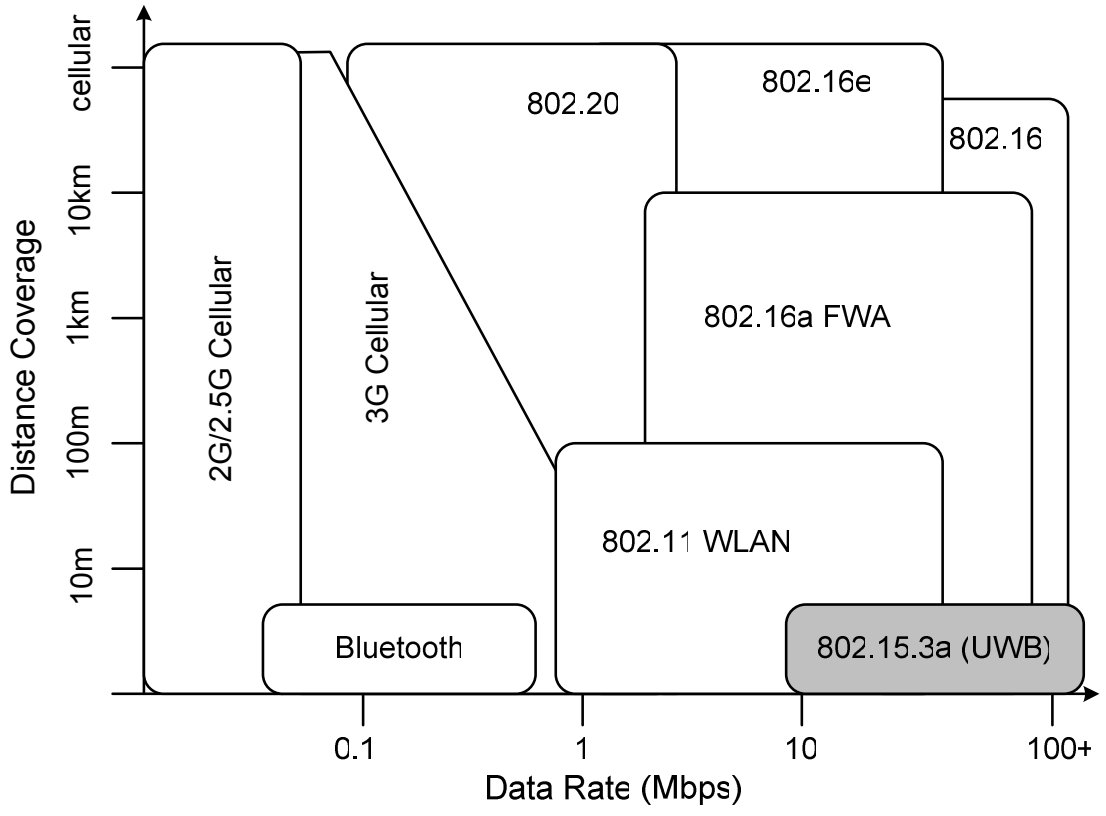

Figure 1.3 Operation distance and data rate of major wireless standards.

A comparison between a basic UWB transceiver and a conventional narrowband transceiver is shown in Figure 1.4. The main difference between them is the saving of the complex superheterodyne structure in a UWB transceiver. The transmission of UWB waveforms can be free of sine-wave carriers (called "carrier-less short pulse" technique [13]) and do not require any IF processing because they can operate in the baseband.

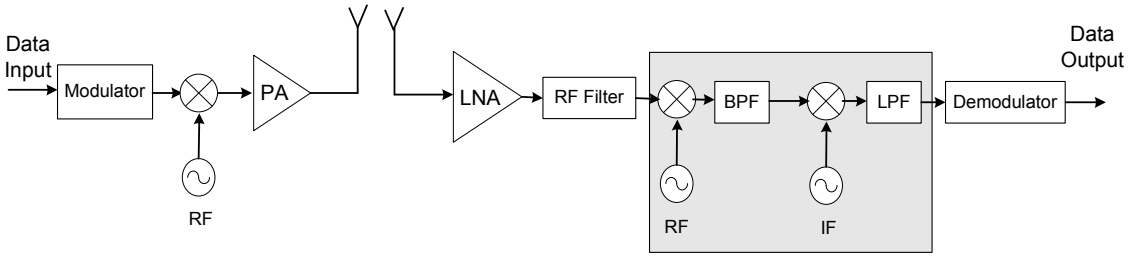

(a) Typical narrowband transceiver architecture

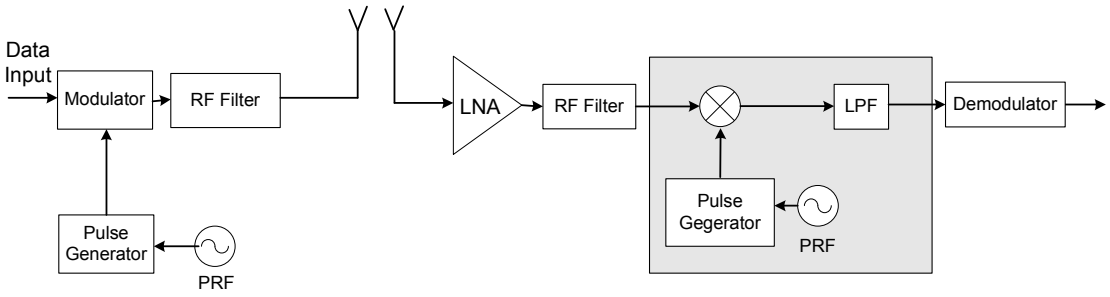

(b) Typical UWB transceiver architecture

Figure 1.4 Comparison of UWB and conventional NB transceiver architectures.

To characterize the UWB propagation channel, many responses have been received to the Call for Contributions on UWB Channel Model [14]. Considering various proposals that optimally chose the respective model parameters (such as mean excess delay, root mean square (RMS) delay, mean number of significant paths etc) to best fit the observed data, the IEEE 802.15.3a channel modeling task group has adopted a modified version of the Saleh-Valenzuela (S-V) model for indoor channels [15]. The channel measurements

showed a clustering of the multipath arrivals which is best captured by the S-V model. More details on the channel model will be discussed in chapter 3. Basically, the very wide bandwidth of the transmitted pulse allows fine resolution of the multipath components. This has both pros and cons. Fine delay resolution implies the potential for significant diversity gains due to the large number of available paths. However, the total received energy is distributed over a large number of paths, which means the receiver must be capable of picking up and combining the multipath energy in a proper way. Normally a Rake receiver is employed for this job.

In summary, occupying huge bandwidth by transmitting ultra short (in nanosecond scale) information-baring pulses, UWB radio has unique advantages that have long been appreciated by the radar and communications communities:

- The wide bandwidth and high time resolution ability of UWB signals generally make them more robust to multipath interference and channel fading;
- A direct application of the Shannon's capacity theorem to an additive white Gaussian noise (AWGN) channel shows that UWB systems offer a potentially high data rate transmission capability with capacity increasing linearly with bandwidth;
- The low transmission power of the UWB signals translates into a RF signature with a low probability of interception and detection (LPI/LPD), and also produces minimal interference to proximity systems and minimal RF health hazards;
- The fine time resolution of UWB systems makes them good candidates for

location and ranging applications (with precision at the centimeter level); and

- More importantly, UWB systems have low system complexity and low cost, since they are essentially baseband systems and can be made nearly "all-digital", with minimal RF or microwave electronics.

1.2 Scope of the Thesis

The whole project is funded and supported by the Agency of Science, Technology and Research (A-STAR) UWB Research program, jointly collaborated between Institute of Microelectronics (IME) of Singapore and National University of Singapore (NUS).

The target of this thesis is to develop a practical and effective algorithm for low complexity receivers of Impulse Radio (IR) UWB communication systems. The theoretical performance analysis is carried out in details with a closed form bit error rate (BER) expression derived. Extensive simulations have been done to verify the correctness of the derivation.

The BER performance of the proposed architecture is also compared with conventional Rake receivers to demonstrate its feasibility of implementations.

1.3 Organization of the Thesis

In chapter 1, the background of UWB communication systems is briefly introduced. Chapter 2 presents some relevant works which have been done so far in this area. Two normal UWB transmission schemes, IR and Multi-Band Orthogonal Frequency Division Multiplexing (MB-OFDM), are described. Common Rake receiver structure is also given in this chapter. The novel blind Rake (BRake) algorithm is proposed in chapter 3 with detailed explanations on the signal model, channel model and receiver structure, followed by in-depth performance analysis in chapter 4. Chapter 5 shows the simulation results which have verified the theoretical derivation, as well as compared the performance of the proposed algorithm and conventional methods. Conclusion remarks are given in chapter 6 with suggested future work.

2 LITERATURE REVIEW

This chapter reviews some of the related literature works. Direct Sequence (DS) and Multi-Band Orthogonal Frequency Division Multiplexing (MB-OFDM) are the two mostly employed UWB transmission techniques. Impulse Radio (IR) is the simplest and most frequently adopted form of DS-UWB, therefore it is the focus of this investigation. MB-OFDM has a major advantage in flexible spectrum selection, but the transceiver structure is complicated due to the presence of multiple frequencies. IR, on the other hand, operates in the baseband and does not require any IF processing, which results in much simplified receiver structure. Therefore IR scheme is adopted in this thesis. The impulse shape and signal modulations of IR-UWB are then reviewed. The second order derivative Gaussian monocycle and BPSK are chosen in our system.

Common Rake receiver structure is also reviewed in this chapter. Rake receivers are used to capture multipath dispersed channel energy in wireless communication systems. All Rake (ARake), Selective Rake (SRake) and Partial Rake (PRake) are commonly known Rake types. Performance and complexity are trade-offs in considering using different types of Rake structures. Channel state information (CSI) has to be provided for Rake receivers to work effectively, but UWB channels are very difficult and costly to be estimated in real time. This is why our BRake structure is proposed and developed.

2.1 IR & MB-OFDM

There are different ways of utilizing the 7.5 GHz bandwidth assigned by FCC in UWB systems. On one hand, the signal can be shaped so that its envelope expands the full frequency spectrum. This is called IR-UWB [6]-[8], [25], also known as pulsed UWB, and it is one of the simplest forms of DS-UWB. On the other hand, the huge band can be divided into multiple subbands, and the signal can be shaped so that it occupies a subband of 500-800 MHz. This is called multiband UWB (MB-UWB) [16]-[18]. With the formation of the Multi-Band OFDM Alliance (MBOA) in June 2003, the OFDM technique for each subband was added to the initial multiband approach to improve the performance due to OFDM's inherent robustness to multipath [19], [20].

The MB-OFDM approach allows for adaptation to different regulatory environments by dynamically turning off subbands and individual OFDM tones to comply with local rules of operation on allocated spectrum. It also facilitates future scalability of the spectrum use.

The band plan for the MBOA proposal is shown in Figure 2.1. The available spectrum of 7.5 GHz is divided into 14 subbands each of 528 MHz. Subbands are grouped into five logical channels. Channel 1, which contains the first three bands, is mandatory for all UWB devices and radios while the other remaining channels are optional. There are up to four time-frequency codes (TFC) per channel, thus allowing for a total of 20 piconets with the current MBOA proposal. In addition, the proposal also allows flexibility to avoid channel 2 when and if Unlicensed National Information Infrastructure (U-NII) interference, such as from 802.11a, is present [21].

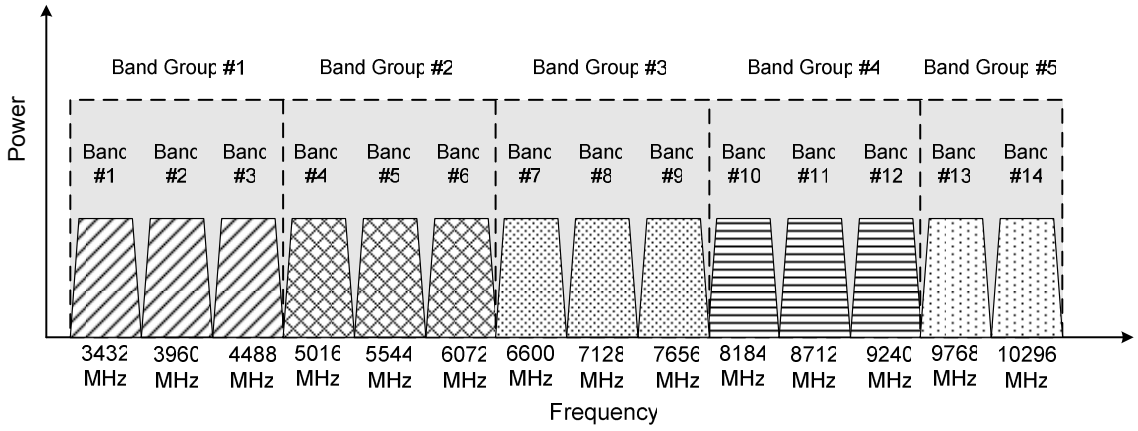

Figure 2.1 The MB-OFDM frequency band plan.

The information transmitted on each subband is modulated using OFDM. OFDM technique distributes the data over a large number of carriers that are spaced apart at precise frequencies. This spacing provides the orthogonality property which prevents the demodulators from seeing frequencies other than their own. The benefits of OFDM are high-spectral efficiency, resiliency to RF interference, and lower multipath distortion. Figure 2.2 shows a typical transceiver architecture for an MB-OFDM system.

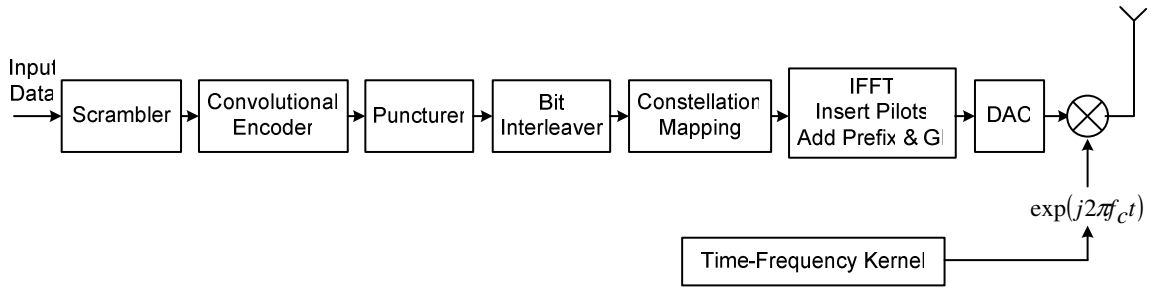

(a) Transmitter structure.

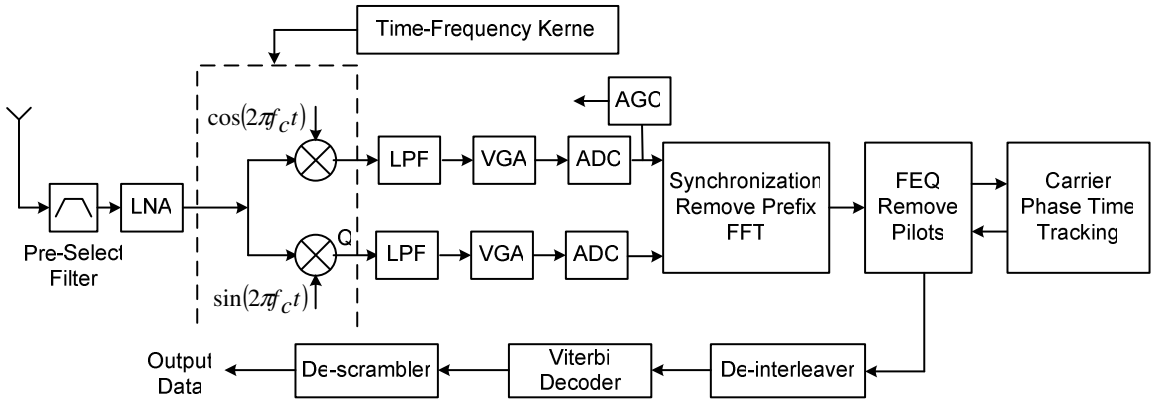

(b) Receiver structure.

Figure 2.2 A typical transceiver architecture for a MB-OFDM system.

The transmitter and receiver architecture for a MB-OFDM system are very similar to those conventional wireless OFDM systems. The main difference is that the MB-OFDM system uses a time-frequency kernel (TFK) to specify the center frequency for the transmission of each OFDM symbol [11].

Despite the above mentioned advantages provided by MB-OFDM scheme, there are also problems associated with this approach. Complicated transceiver architecture is a major concern. Firstly, to generate all the subcarrier frequencies, frequency synthesizer must be built which ensures that system can switch between the center frequencies extremely fast (within a few nanoseconds). Secondly, local oscillators at the UWB transmitter and receiver end are prone to mismatch and give rise to multiple carrier frequency offset/jitter (CFO/CFJ) [22]. Unless compensated for, CFO/CFJ is known to degrade the system performance severely. Thus MB-OFDM needs for CFO sensitivity analysis, low complexity CFO estimators, and per-subcarrier based channel estimation modules. Lastly, the additional IFFT/FFT modules in the transceiver systems add about 25% of the digital

baseband processing complexity, which also results in more power consumption.

IR scheme, on the other hand, avoids using sinusoidal carriers or any IF processing so that it greatly reduces the transceiver complexity and overall power consumption. Therefore it is adopted in our system with its simpler transceiver architecture.

IR works by transmitting baseband pulses of very short duration, typically on the order of nanosecond or sub-nanosecond, thereby spreading the energy of the radio signal very thinly from near DC to a few gigahertzes [8]. The shape of the pulse specifies the frequency spectrum of the transmitted signal and well designed pulse shape allows maximum emitted power under FCC frequency mask. A variety of pulse shapes and their corresponding frequency spectrums have been proposed and discussed in [23]-[28]. Among them, the most frequently employed pulse shapes are the derivatives of Gaussian function. The time domain and frequency domain representations of the n^{th} order Gaussian derivative $p_n(t)$ and $P_n(f)$ are given in (2.1) and (2.2) [28], respectively,

$$p_n(t) = (-1)^{\lfloor (3n+1)/2 \rfloor} n! \pi^{-1/4} e^{-\left(\frac{1}{2\sigma^2}\right)t^2} \times \sum_{k=0}^{\lfloor n/2 \rfloor} \frac{(-1)^k 2^{n+1/4-2k} \left(\frac{1}{2\sigma^2}\right)^{n/2+1/4-k} t^{n-2k}}{(n-2k)!k!\sqrt{(2n-1)!!}}, \quad (2.1)$$

where $(2n-1)!! = (2n-1)\cdot(2n-3)\cdot\ldots\cdot 3\cdot 1$, σ is the standard deviation of the Gaussian function which is associated with the pulse duration.

$$P_n(f) = \frac{(-1)^n i^{n^2} (2\pi)^{n+1/4} \left(2\sigma^2\right)^{n/2+1/4}}{\sqrt{(2n-1)!!}} f^n e^{-2\pi^2 f^2 \sigma^2}. \quad (2.2)$$

where i represents the imaginary part of a complex number.

Figure 2.3 shows the waveforms of 1st order to 4th order derivative Gaussian monocycles and their corresponding power spectrums. It can be seen that increasing the derivative order of the Gaussian monocycle has the effect of shifting the frequency spectrum to occupy a higher frequency range so that it can better fit FCC frequency mask. However higher order derivative monocycle is not feasible from circuit perspective as well as mathematical tractability. In this thesis, a commonly used 2nd order Gaussian monocycle is employed with pulse duration of $T_p = 0.25$ ns. The impulse can be written as, in a simplified version from (2.1):

$$g(t) = A\left[1 - \left(\frac{t}{\sigma} - 3.5\right)^2\right] e^{-0.5\left(\frac{t}{\sigma} - 3.5\right)^2}, \tag{2.3}$$

where σ is related to the pulse width by $T_p = 7\sigma$ with T_p being the duration of a single pulse which covers 99.99% of the total pulse energy, and A is a factor to normalize the pulse energy to one.

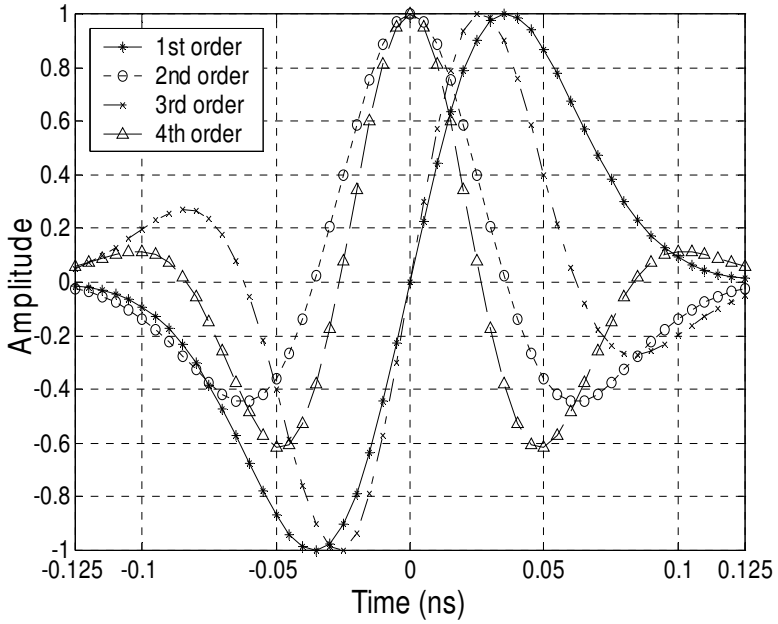

(a) Time domain derivatives of Gaussian waveform.

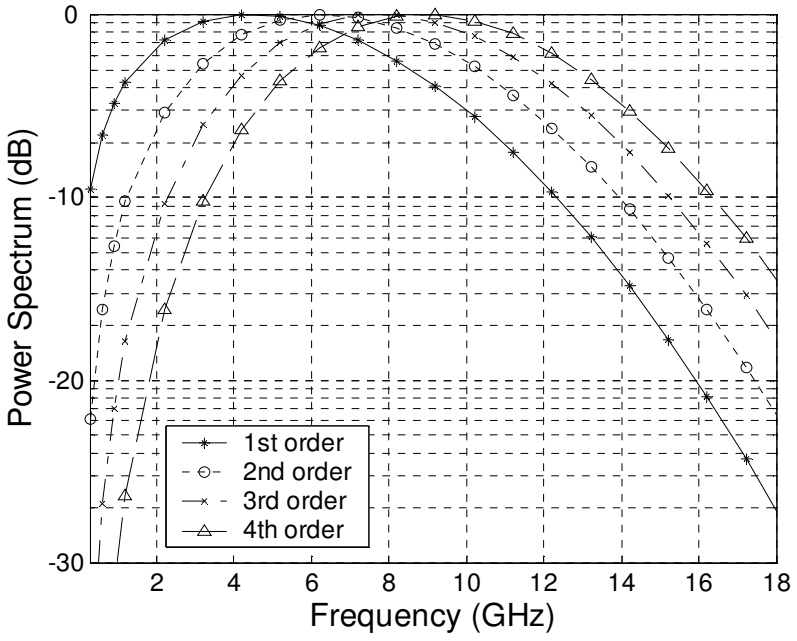

(b) PSD of derivatives of Gaussian waveform.

Figure 2.3 Waveforms for derivatives of Gaussian monocycle.

Three types of modulations are usually employed in IR-UWB systems. They are pulse position modulation (PPM), pulse amplitude modulation (PAM), and binary phase shift keying (BPSK) or biphase modulation [16].

PPM is based on the principle of encoding information with two or more positions in time, referred to the nominal pulse position, as shown in Figure 2.4 (a). The graph shows 2-PPM, where one bit is encoded in one impulse. Additional positions can be used to provide more bits per symbol. The time delay between positions is typically a fraction of a nanosecond, while the time delay between nominal positions is called pulse repetition time (PRT), T_{pr} in the graph, and it is much longer to avoid interference between impulses. PPM was mostly adopted in the early development of UWB radios when negating ultra short pulses were difficult to implement [22].

PAM is based on the principle of encoding information with the amplitude of the impulses, as shown in Figure 2.4 (b). The graph shows 2-PAM, and more bits can be provided per symbol by using more levels of different amplitudes.

In BPSK or biphase modulation, information is encoded with the polarity of the impulses, as can be seen in Figure 2.4 (c). In a more general sense, BPSK can also be regarded as a special case of a 2-PAM.

Other modulation techniques have also been explored [29], [30] and they are basically derived or combined from the above mentioned three basic types.

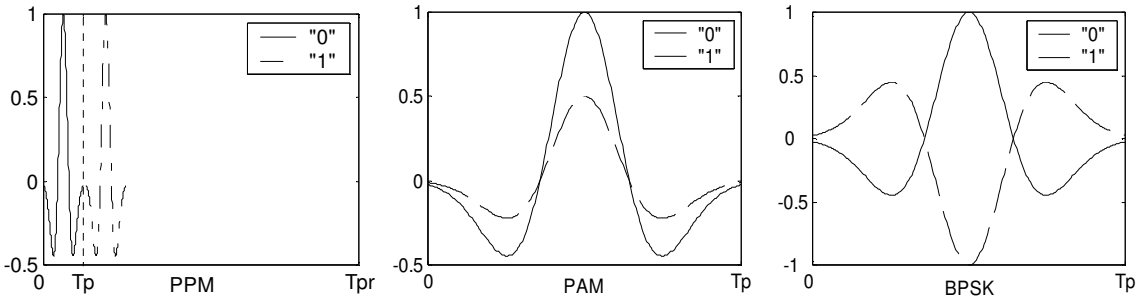

(a) PPM (b) PAM (c) BPSK

Figure 2.4 IR-UWB modulations.

IR-UWB transmits information by sending extremely short pulses with low duty cycle, so the transmitted power can be small. It requires no carrier modulation and RF power amplifier which results in simple architecture. Its fine time resolution property makes it robust to multipath fading. To effectively explore the channel diversity, a Rake receiver is usually employed at the receiver end.

2.2 Rake Receiver

In a typical wireless environment, an electromagnetic (EM) wave traverses a multitude of paths from the transmitter to the receiver, whose lengths are unequal in general due to deflections, reflections and scatterings. The composite signal at receiver side is the superposition of time shifted, amplitude scaled, polarization rotated and phase altered copies of the transmitted signal, and it is called multipath distorted. The exact number of multipaths depends on the geometry of the environment, the location of the transceivers, the placement of the obstructive and non-obstructive objects, and the properties of materials used in construction. In general the channel impulse response (CIR) of a multipath fading channel can be modeled as:

$$h(t) = \sum_{m=1}^{M} \alpha_m \delta(t - \tau_m), \tag{2.4}$$

where α_m and τ_m represent the channel attenuation and the propagation delay of the m^{th} multipath component and they are referred to as channel state information (CSI). $\delta(\cdot)$ is the Dirac delta function. M represents the total number of multipath components and usually $M \to \infty$. The channel amplitude response is normalized such that:

$$\sum_{m=1}^{M} \alpha_m^2 = 1. \tag{2.5}$$

Let $s(t)$ represent the transmitted signal, then the received signal after passing through the multipath channel is:

$$r(t) = s(t) \otimes h(t) + w(t)$$

$$= \sum_{m=1}^{M} \alpha_m s(t-\tau_m) + w(t), \tag{2.6}$$

where $w(t)$ is AWGN with two side power density $\frac{N_0}{2}$. This expression indicates that the signal energy is dispersed in M multipath components.

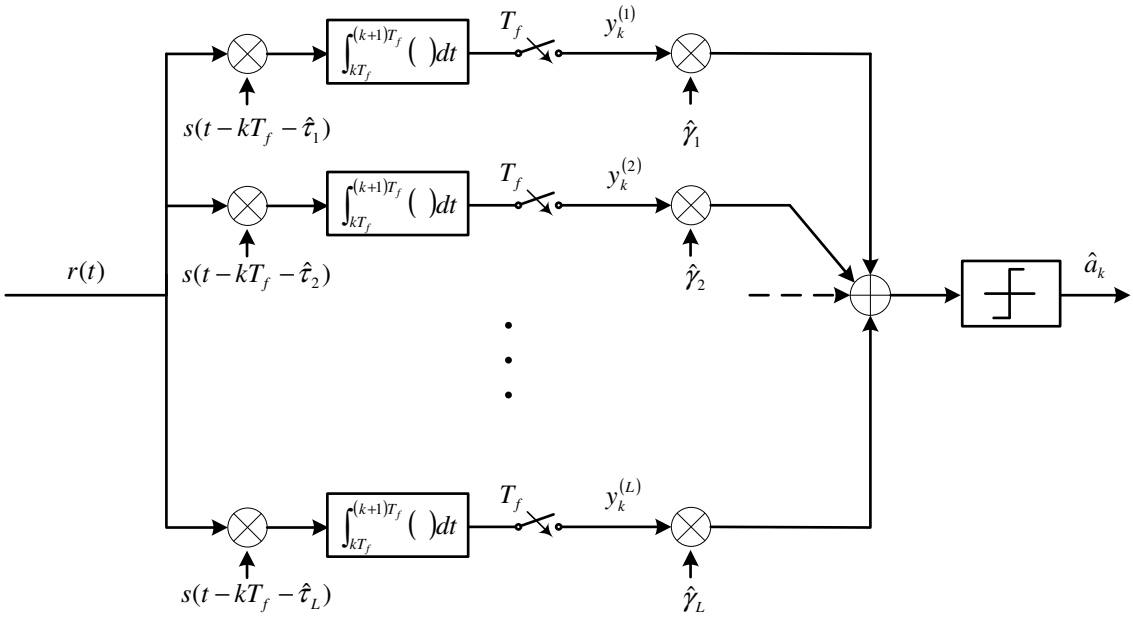

Figure 2.5 A general Rake receiver structure.

A general Rake structure is shown in Figure 2.5. It consists of multiple fingers (correlators) where each finger can extract one of the multipath components provided by the channel. The outputs of all the fingers are appropriately weighted and combined to provide the multipath diversity. The equivalent matched filter (MF) version of the receiver involves a matched front-end processor (MFEP) (matched only to the transmitted waveform) followed by a tapped delay line (TDL) and a combiner [31]. The MFEP resolves multipath components whose delays differ by at least one chip duration, T_c,

approximately equal to the inverse of the spreading bandwidth. The output of MFEP is passed through a TDL filger with L taps, which are combined with maximum ratio combing (MRC) for the best possible performance.

The ideal SNR at the output of Rake receiver is given by [31]:

$$\gamma = \frac{E_b}{N_0 / 2} \sum_{m=1}^{M} \alpha_m^2 , \tag{2.7}$$

where E_b is the bit energy of the transmitted signal. With $\sum_{m=1}^{M} \alpha_m^2 = 1$, (2.7) recovers the largest possible SNR of the received signal. The BER performance is shown to be [30]:

$$P_b = Q\left(\sqrt{SNR}\right) = Q\left(\sqrt{\gamma}\right), \tag{2.8}$$

where $Q(\cdot)$ is the complementary cumulative distribution function.

An ideal Rake is referred to as all Rake (ARake), which indicates the receiver with unlimited resources and instant adaptability so that it can resolve all the multipath components. To achieve this, it requires $L = T_d / T_c$ correlators/taps, where T_d is the maximum excess delay. There are hundreds of multipath components in a typical UWB channel. Therefore ARake is unrealistic due to the power consumption, design complexity and channel estimation [32]. It can only serve as a benchmark that provides an upper limit to the achievable performance.

Selective Rake (SRake) and partial Rake (PRake) are two commonly employed complexity-reduced Rake structures which process only a subset of available L multipath

components. SRake selects the L_b best (with largest instantaneous SNR) out of L total multipath components and combines them using MRC [33]-[35], while PRake has L_p fingers that tract the first L_p paths arrived at the receiver [36], [44]. SRake requires fast adaptability, knowledge of instantaneous values of all multipaths and efficient channel estimation, and is therefore more complex than PRake.

Systems employing various types of Rake structures and their performances have been reported [20], [33]-[46]. However Rake implementation can be effective only when the CSI is available or can be properly estimated at the receiver. This poses a major problem in UWB communications, since even if we opt to utilize only a few (e.g. five strongest out of hundreds of) paths, accurate estimation of the five strongest channel gains and their corresponding delays is required.

Channel estimation has long been a challenge in UWB systems. Impulse response estimator for UWB channels has been presented in [13], [47]-[50]. Computational complexity of the ML channel estimator in [13] and [47] increases with increasing number of multipath components, and is unaffordable for realistic UWB channels. Moreover, channel estimators require the ADC to work at over-sampling rate to get the correct estimation of the time delays. With the UWB sub-nanosecond-width impulse, the ADC sampling rate is in the formidable range of over 10 GHz [22] which is very costly.

In this thesis, a low complexity *blind Rake* (*BRake*) structure is proposed, which does not require any CSI yet provides acceptable BER performance. The sampling rate required for the receiver ADC is also greatly reduced.

3 SYSTEM MODEL & RECEIVER DESIGN

The proposed system model and receiver architecture are present in this chapter.

Pulse shaping and modulation of our system is discussed. BPSK is adopted for the sake of mathematical simplification.

IEEE 802.15.3a multipath indoor channel models are employed and the large number of multipaths is observed.

The BRake receiver structure is then proposed. It consists of multi branches of Rake fingers and each branch is sampled at different rates. The receiver model parameters are chosen based on channel delay profiles.

3.1 Pulse-shaping & Modulation

As discussed in chapter 2, the 2nd order derivative of a Gaussian pulse, $g(t)$ given in (2.3), is adopted in our system design since it is one of the mostly used impulses in IR-UWB and it can be easily generated for simulation. However the algorithm presented in this thesis is also applicable to other pulse shapes.

In general, the transmitted waveform of an IR-UWB system is given by [22]:

$$s(t) = \sqrt{E_p} \sum_{n=0}^{+\infty} b_{\lfloor n/N_f \rfloor} \cdot g\left(t - nT_f - c_n^{TH} T_c - d_{\lfloor n/N_f \rfloor} \Delta\right), \tag{3.1}$$

where E_p is the pulse energy at the transmitter end. To increase SNR at the receiver end, each symbol is represented by N_f replicas, each replica transmitted per frame of duration $T_f >> T_p$. T_f is also knows as PRT. For multi-user access (MA), c_n^{TH} represents the user-specific time hopping (TH) code. Every frame is divided into N_c chips with each of duration T_c, and $c_n^{TH} T_c$ corresponds to a time shift during the n^{th} frame. With $m_k \in [0, M-1]$ denoting the M-ary information symbol transmitted during k^{th} symbol duration, (3.1) subsumes PPM and PAM. When $d_k = m_k$ and $b_k = 1$, (3.1) models M-ary PPM for UWB transmissions, and $d_k \Delta$ is the pulse position offset. When $b_k = 2m_k - M + 1$ and $d_k = 0$, (3.1) describes M-ary PAM.

To simplify the analysis in this thesis, single user environment is considered ($c_n^{TH} = 0$) and BPSK ($d_{\lfloor n/N_f \rfloor} = 0$) modulation is employed in our system. Moreover, each symbol is

transmitted by one pulse to increase the transmission rate ($N_f = 1$). Then the transmitted sequence is much simplified from (3.1) and can be written as:

$$s(t) = \sqrt{E_p} \sum_{n=0}^{+\infty} b_n g\left(t - nT_s\right), \tag{3.2}$$

where $b_n \in \{\pm 1\}$ is the binary data transmitted and T_s represents the bit duration. The quantity $\phi = \frac{T_s}{T_p}$ is called the processing gain and should be much greater than 1 to minimize the inter symbol interference (ISI). At the same time, transmission rate decreases with increasing ϕ. Thus compromise must be made between performance and capacity.

Although the performance analysis in this thesis is carried out using BPSK modulation, the results can be easily extended to PPM or other modulation schemes.

3.2 Multipath Channel Model

Since most of the envisioned UWB commercial applications will be indoor communications, UWB indoor channels are considered in this thesis. The IEEE 802.15.3a Task Group proposed an indoor channel model which is a modified version of the well know Saleh-Valenzuela (S-V) model in November 2002 [14].

S-V indoor channel model was established in 1987 based on measurements utilizing low power ultra-short pulses of width 10 ns and center frequency 1.5 GHz in a medium size, two-story office building [15]. Multipath components arrive at the receiver in groups (clusters) in this model. Multiple rays are observed within each cluster. The cluster and ray arrivals are both Poisson distributed. Rayleigh distribution is assumed for the multipath gain magnitude with an exponentially decaying power profile.

The clustering phenomenon has been experimentally confirmed in characterizing UWB indoor channels. Thus UWB indoor channel models are derived from S-V model with a couple of slight modifications. A lognormal distribution rather than a Rayleigh distribution for the multipath gain is adopted since it fits the measurement data better [14]. In addition, independent fading is assumed for each cluster as well as each ray within the cluster. The multipath channel model is therefore expressed as [14]:

$$h(t) = X \sum_{l=0}^{L} \sum_{k=0}^{K} \alpha_{k,l} \delta\left(t - T_l - \tau_{k,l}\right), \tag{3.3}$$

where X is the log-normal shadowing, $\alpha_{k,l}$ is the multipath gain coefficient of the k^{th} multipath of the l^{th} cluster, T_l is the delay of the l^{th} cluster and $\tau_{k,l}$ is the delay of k^{th}

multipath component relative to the l^{th} cluster arrival time. Cluster and ray arrivals are independent Poisson distributed with rate Λ and λ, respectively, and $\lambda > \Lambda$. The total number of paths is defined as the number of multipath arrivals with expected power within 10 dB from that of the strongest arrival path.

The detailed UWB multipath channel characteristics and parameters for channel model 1 to channel model 4 (CM1-CM4) are provided in [14].

Typical realizations of the channel impulse response generated for CM1-CM4 are shown in Figure 3.1.

It can be seen that the multipath components for each type of the channel are enormous. For CM3 and CM4, there are even more multipaths present and the dispersed channel length is also longer than that for CM1 and CM2.

When doing performance analysis in chapter 4, the simplified CIR model given in (2.4) is adopted instead of (3.3), and the channel is viewed as consisting of M discrete time impulse responses.

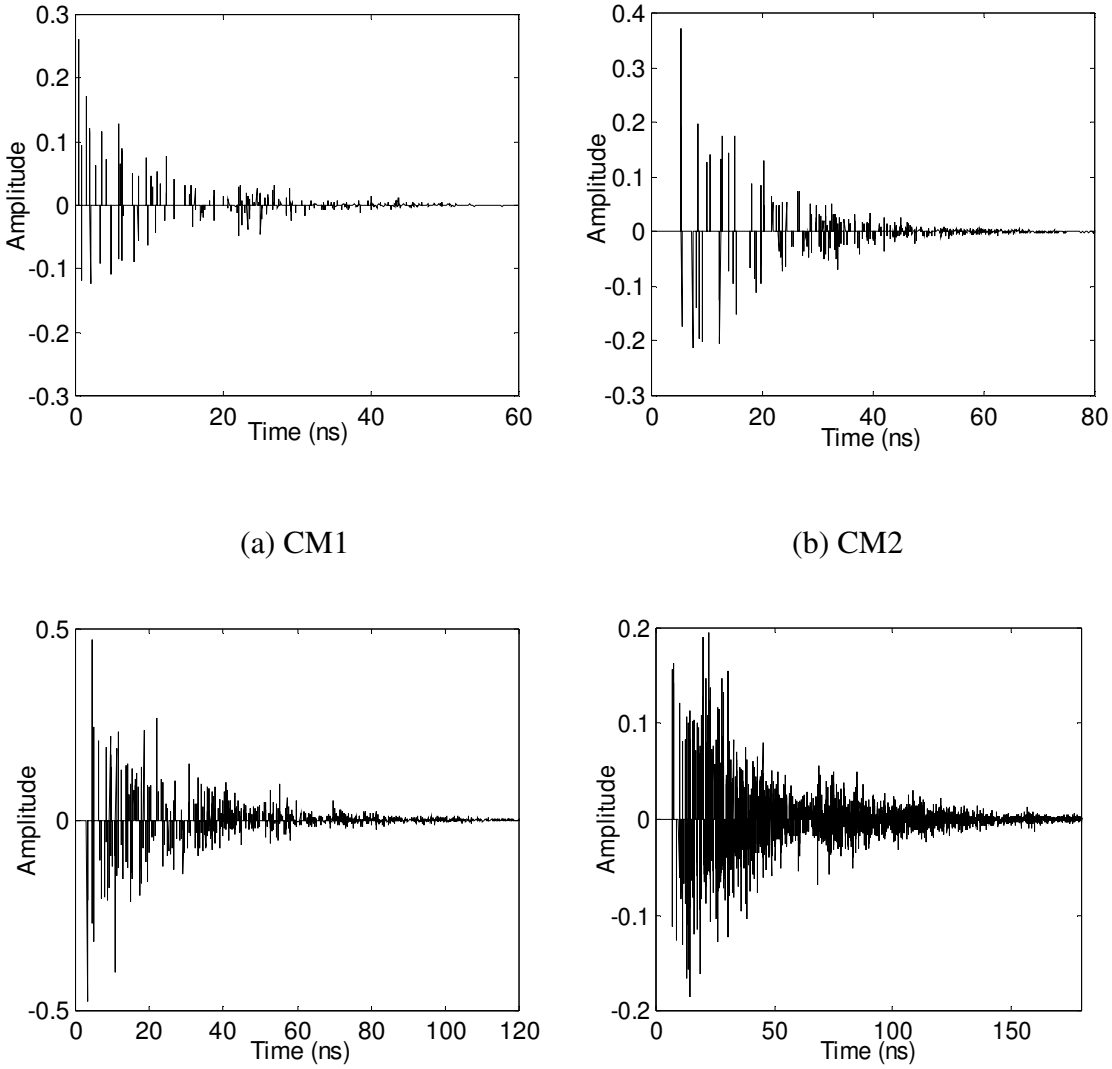

(a) CM1

(b) CM2

(c) CM3

(4) CM4

Figure 3.1 Typical CIRs for UWB indoor channels.

3.3 BRake Receiver Structure

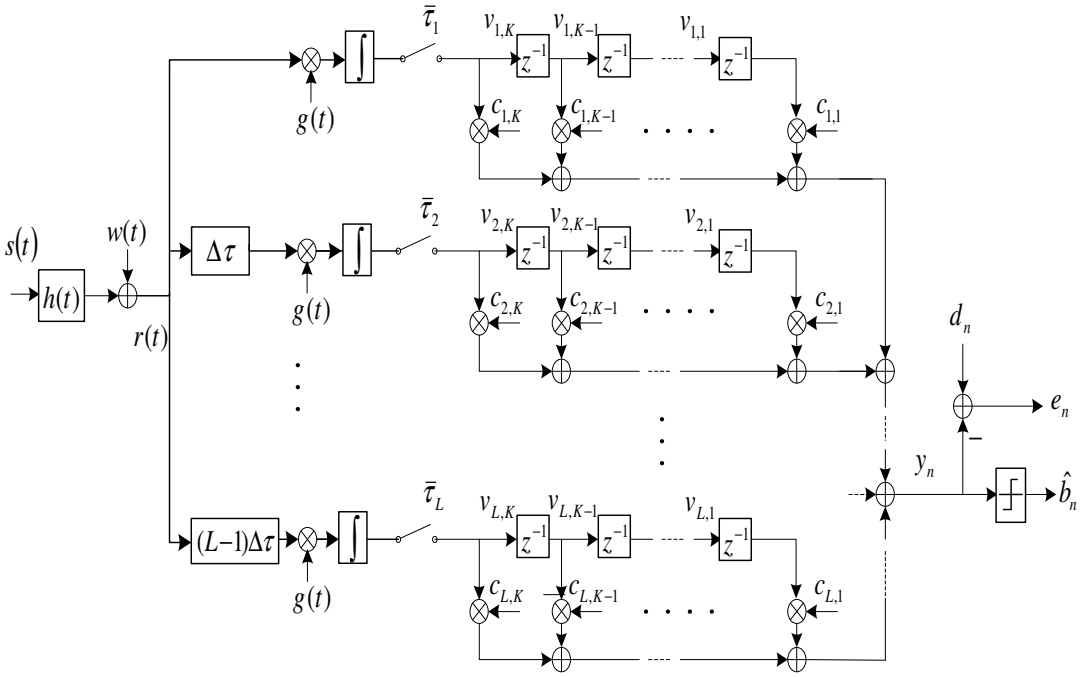

Figure 3.2 BRake receiver architecture.

The proposed BRake receiver structure is shown in Figure 3.2. It consists of L branches with K taps in each branch. The received signal $r(t)$ is delayed by a small time $\Delta\tau$ in each consecutive branch to ensure that the receiver does not sample at the same time instance. After that the signal is correlated with a locally generated pulse $g(t)$ and then sampled at different rates in every branch. Each branch represents a BRake branch with a unique sampling interval $\bar{\tau}_l \in \{\bar{\tau}_1, \bar{\tau}_2, \ldots, \bar{\tau}_L\}$, $\bar{\tau}_1 < \bar{\tau}_2 < \ldots < \bar{\tau}_L$, where the fastest sampling rate $\frac{1}{\bar{\tau}_1}$ is well below the Nyquist rate. The sampled data are properly weighted by the tap coefficients $\{c_{1,1}, c_{1,2}, \ldots, c_{1,K}, c_{2,1}, c_{2,2}, \ldots, c_{2,K}, \ldots, c_{L,K}\}$ and summed up to form the decision signal y_n. The decision rule is:

$$\hat{b}_n = \begin{cases} 1 & if\ y_n > 0 \\ -1 & if\ y_n < 0 \end{cases}. \tag{3.4}$$

During the training phase, the TDL coefficient set $\{c_{l,k}\}$ is updated adaptively using the least mean square (LMS) method [51]:

$$e_n = d_n - y_n, \tag{3.5}$$

$$c_{n+1}^{l,k} = c_n^{l,k} + 2\mu e_n v_n^{l,k}, \tag{3.6}$$

where d_n represents the n^{th} desired signal, e_n represents the n^{th} error, $c_n^{l,k}$ represents the n^{th} adaptation value of tap $c_{l,k}$, $l \in \{1, 2, \ldots, L\}$, $k \in \{1, 2, \ldots, K\}$, and $v_n^{l,k}$ is input of the k^{th} tap in the l^{th} branch for symbol n.

After $\{c_{l,k}\}$ converge to their optimum values, the algorithm will exam the pattern of the tap values. There are certain taps that do not sample at any correct time instance of the multipath, and these tap values converge to very small numbers near zero. Thus they can be discarded since including them only adds the noise component and consumes more hardware. On the other hand, when the tap happens to sample at the correct time instance of any multipath, the tap value will converge to the channel attenuation value corresponding to that delay time, and the successfully sampled energy will be counted into the decision signal. More details on this will be revealed in the next 2 chapters.

From the proposed structure and algorithm, it can be calculated that the total sampling interval for each received data bit is $(L-1)\Delta\tau + (K-1)\overline{\tau}_L$. The choice of L, K, $\{\overline{\tau}_1, \overline{\tau}_2, \ldots, \overline{\tau}_L\}$ and $\Delta\tau$ are closely related to the channel profile. Referring to the power

delay profile (PDP) of CM1-CM4, it is found that the channel multipath components and energy reduce exponentially with time delay [14]. Thus it makes sense to sample at a reduced rate for consecutive branches, i.e., $\bar{\tau}_1 < \bar{\tau}_2 < \ldots < \bar{\tau}_L$. At the same time, the total sampling interval should cover most of the dispersed channel energy. The RMS delay spread, defined as the second centered moment of the delay spectrum of a stochastic channel, is commonly used to describe a dispersed channel PSD:

$$\tau_{RMS} = \sqrt{\sigma_\tau^2} = \overline{\overline{\tau^2}} - \left(\bar{\tau}\right)^2, \tag{3.7}$$

where $\overline{\overline{\tau^n}} = \dfrac{\int_{-\infty}^{+\infty} \tau^n S_{\tilde{h}}(\tau) d\tau}{\int_{-\infty}^{+\infty} S_{\tilde{h}}(\tau) d\tau}$ and $S_{\tilde{h}}(\tau)$ is the delay spectrum. The RMS delay spread for CM1-CM4 is 5 ns, 8 ns, 14 ns, and 26 ns [14], respectively. As a suggestion, it may be set:

$$\bar{\tau}_{i+1} = \xi_1 \bar{\tau}_i, i = 1,2,\ldots L-1,\ 1.1 < \xi_1 < 1.5, \tag{3.8}$$

and

$$(L-1)\Delta\tau + (K-1)\bar{\tau}_L = \xi_2 \tau_{RMS},\ 2.5 < \xi_2 < 4. \tag{3.9}$$

According to our investigation and simulation, the above suggested range of ξ_1 and ξ_2 can achieve good BER performance by capturing enough multipath energy.

4 PERFORMANCE ANALYSIS

Thorough performance analysis of the proposed receiver is carried out in this chapter.

Firstly correlation receivers are discussed because Rake structure consists of a number of correlators.

To determine the optimum tap weights, Minimum Mean Square Error (MMSE) criterion is adopted and Wiener solution is derived based on this.

However, the tap weights obtained practically are adapted using LMS technique, where there is an additional error term associated with the adaptation step size.

The output SNR is then derived considering the LMS error, from which the final BER expression is obtained.

4.1 Correlation Receivers

The Rake structure is used to produce a weighted sum of the outputs from a set of correlation receivers. So the performance analysis begins with the signal passing through the correlation receivers.

Referring to Figure 3.2, some vectors are defined which will appear in this chapter:

Training sequence:

$$\mathbf{b_n} = [b_0\ b_1 \ldots\ b_{N-1}\ ]^T; \tag{4.1}$$

Channel attenuations:

$$\boldsymbol{\alpha}_\mathbf{m} = [\alpha_1\ \alpha_2 \ldots\ \alpha_M\ ]^T; \tag{4.2}$$

Channel delays:

$$\boldsymbol{\tau}_\mathbf{m} = [\tau_1\ \tau_2 \ldots\ \tau_M\ ]^T; \tag{4.3}$$

Receiver sampling times:

$$\boldsymbol{\tau}_\mathbf{lk} = [\bar{\tau}_{1,1}\ \bar{\tau}_{1,2}\ \ldots\ \bar{\tau}_{L,K}\ ]^T, \tag{4.4}$$

where $\bar{\tau}_{l,k}, l = 1,2\ldots L, k = 1,2\ldots K,$ represents the sampling time of the k^{th} tap in the l^{th} branch;

Gaussian pulse vector based on real channel timing:

$$\mathbf{g_m} = [g(t - nT_s - \tau_1)\ g(t - nT_s - \tau_2) \ldots\ g(t - nT_s - \tau_M)]^T; \tag{4.5}$$

Gaussian pulse vector based on receiver sampling timing:

$$\mathbf{g_{l,k}} = [g(t - nT_s - \bar{\tau}_{1,1})\ g(t - nT_s - \bar{\tau}_{1,2}) \ldots\ g(t - nT_s - \bar{\tau}_{L,K})]^T; \tag{4.6}$$

Tap weight:

$$\mathbf{c} = [c_{1,1}\ \ c_{1,2}\ \ \ldots\ c_{1,K}\ \ c_{2,1}\ \ c_{2,2}\ \ \ldots\ \ c_{2,K}\ \ \ldots\ \ c_{L,K}\ ]^T. \tag{4.7}$$

From (2.4), (2.6) and (3.2), the received signal $r(t)$ can be expressed as:

$$\begin{aligned} r(t) &= s(t) \otimes h(t) + w(t) \\ &= \sqrt{E_p} \sum_{n=0}^{+\infty} b_n g(t - nT_s) \otimes \sum_{m=1}^{M} \alpha_m \delta(t - \tau_m) + w(t) \\ &= \sqrt{E_p} \sum_{n=0}^{+\infty} b_n \sum_{m=1}^{M} \alpha_m g(t - nT_s - \tau_m) + w(t). \end{aligned} \tag{4.8}$$

Due to the low duty cycle property of IR-UWB transmissions, it is reasonable to assume that there is no ISI present. For simplification of analysis, the waveform for detection of the n^{th} symbol can be written as:

$$r_n(t) = \sqrt{E_p} b_n \sum_{m=1}^{M} \alpha_m g(t - nT_s - \tau_m) + w(t) = \sqrt{E_p} b_n \boldsymbol{\alpha}_\mathbf{m}^\mathbf{T} \mathbf{g_m} + w(t). \tag{4.9}$$

After the pulse correlator and ADC sampling, the k^{th} tap input of the l^{th} branch is:

$$\begin{aligned} v_{l,k} &= \int_{nT_s + \bar{\tau}_{l,k}}^{nT_s + \bar{\tau}_{l,k} + T_p} r_n(t) g(t - nT_s - \bar{\tau}_{l,k}) dt \\ &= \int_{nT_s + \bar{\tau}_{l,k}}^{nT_s + \bar{\tau}_{l,k} + T_p} \sqrt{E_p} b_n \boldsymbol{\alpha}_\mathbf{m}^\mathbf{T} \mathbf{g_m} g(t - nT_s - \bar{\tau}_{l,k}) dt \end{aligned}$$

$$+\int_{nT_s+\bar{\tau}_{l,k}}^{nT_s+\bar{\tau}_{l,k}+T_p} w(t)g\left(t-nT_s-\bar{\tau}_{l,k}\right)dt$$

$$=\sqrt{E_p}b_n\alpha_{l,k}R_g\left(\bar{\tau}_{l,k}-\tau_m\right)+w_{l,k}, \tag{4.10}$$

where

$$R_g\left(\bar{\tau}_{l,k}-\tau_m\right)=\int_{nT_s+\bar{\tau}_{l,k}}^{nT_s+\bar{\tau}_{l,k}+T_p} g\left(t-nT_s-\tau_m\right)g\left(t-nT_s-\bar{\tau}_{l,k}\right)dt, \tag{4.11}$$

and $w_{l,k}$ is the additive noise after correlation operation. Its power can be calculated as:

$$\begin{aligned}
\sigma_{w_{l,k}}^2 &= E\left[w_{l,k}w_{l,k}^{'}\right] \\
&= E\left[\int_{nT_s+\bar{\tau}_{l,k}}^{nT_s+\bar{\tau}_{l,k}+T_p} w(t)g\left(t-nT_s-\bar{\tau}_{l,k}\right)dt\cdot\int_{nT_s+\bar{\tau}_{l,k}}^{nT_s+\bar{\tau}_{l,k}+T_p} w(t')g\left(t'-nT_s-\bar{\tau}_{l,k}\right)dt'\right] \\
&= \int_{nT_s+\bar{\tau}_{l,k}}^{nT_s+\bar{\tau}_{l,k}+T_p} E\left[w(t)^2\right]g^2\left(t-nT_s-\bar{\tau}_{l,k}\right)dt \\
&= \frac{N_0}{2}\int_{nT_s+\bar{\tau}_{l,k}}^{nT_s+\bar{\tau}_{l,k}+T_p} g^2\left(t-nT_s-\bar{\tau}_{l,k}\right)dt \\
&= \frac{N_0}{2}R_g(0).
\end{aligned} \tag{4.12}$$

Thus $w_{l,k}$ is Gaussian distributed with zero mean and two side power density $\frac{N_0}{2}R_g(0)$, i.e., $w_{l,k} \sim N\left(0,\frac{N_0}{2}R_g(0)\right)$. Since the pulse energy is normalized, i.e., $R_g(0)=1$, $w_{l,k} \sim N\left(0,\frac{N_0}{2}\right)$.

It is obvious that $R_g\left(\bar{\tau}_{l,k}-\tau_m\right)=0$ when $\left|\bar{\tau}_{l,k}-\tau_m\right|>T_p$, as the pulse duration of $g(t)$ is

T_p. Assume there are I fingers that correctly sample the multipath components out of the $L \times K$ total fingers, then (4.10) can be written as:

$$v_{l,k} = \begin{cases} \sqrt{E_p} b_n \alpha_i R_g(\tilde{\tau}_i) + w_{l,k} & \text{when } \tilde{\tau}_i = \left| \bar{\tau}_{l,k} - \tau_m \right| < T_p \\ w_{l,k} & \text{when } \tilde{\tau}_i = \left| \bar{\tau}_{l,k} - \tau_m \right| > T_p \end{cases}, \tag{4.13}$$

where $\{\alpha_i\}$, $i = 1,2 \ldots I$, is a subset of vector $\boldsymbol{\alpha}_\mathbf{m}$ representing the correctly sampled channel impulse response. Let η represent the successfully collected channel energy ratio:

$$\eta = \sum_{i=1}^{I} \alpha_i^2 R_g^2(\tilde{\tau}_i), \tag{4.14}$$

then the missed channel energy ratio is $1-\eta$. Sort $v_{l,k}$ in order of α_i and constellate to form the input tap vector:

$$\begin{aligned} \mathbf{v} &= \left[\sqrt{E_p} b_n R_g(\tilde{\tau}_1)\alpha_1 + w_1 \quad \sqrt{E_p} b_n R_g(\tilde{\tau}_2)\alpha_2 + w_2 \ \ldots \ \sqrt{E_p} b_n R_g(\tilde{\tau}_I)\alpha_I + w_I \right. \\ &\qquad \left. w_{I+1} \quad w_{I+2} \quad \ldots \quad w_{LK} \right]^T \\ &= \begin{bmatrix} b_n \mathbf{S_I} + \mathbf{W_I} \\ \mathbf{W_{LK-I}} \end{bmatrix}, \end{aligned} \tag{4.15}$$

where:

$$\mathbf{S_I} = \sqrt{E_p} \left[\alpha_1 R_g(\tilde{\tau}_1) \quad \alpha_2 R_g(\tilde{\tau}_2) \ \ldots \ \alpha_I R_g(\tilde{\tau}_I) \right]^T, \tag{4.16}$$

$$\mathbf{W_I} = \left[w_1 \ w_2 \ldots \ w_I \right]^T, \tag{4.17}$$

$$\mathbf{W_{LK-I}} = \left[w_{I+1} \ w_{I+2} \ \ldots \ w_{LK} \right]^T. \tag{4.18}$$

Then the detection signal after weight combing is, expressed in vector form:

$$y_n = \mathbf{c}^{\mathbf{T}}\mathbf{v} \quad . \tag{4.19}$$

4.2 MMSE Criterion & Wiener Solution

To determine the optimum weight vector $\mathbf{c_o}$, MMSE criterion is employed and $\mathbf{c_o}$ can be expressed as:

$$\mathbf{c_o} = \arg\min_{\mathbf{c}} J\,, \tag{4.20}$$

where

$$J = E\left[\left\| d_n - y_n \right\|^2\right], \tag{4.21}$$

represents the mean square error (MSE) cost function.

The well known Weiner solution gives [51]:

$$\mathbf{c_o} = \left(E\left[\mathbf{v}\mathbf{v}^{\mathbf{T}}\right]\right)^{-1} \cdot E\left[d_n \mathbf{v}\right]. \tag{4.22}$$

To solve (4.22), we exam $E\left[\mathbf{v}\mathbf{v}^{\mathbf{T}}\right]$ and $E\left[d_n \mathbf{v}\right]$ separately in the following.

From (4.15), and note that signal and noise (with zero mean) are uncorrelated:

$$\begin{aligned} E\left[\mathbf{v}\mathbf{v}^{\mathbf{T}}\right] &= E\left[\begin{bmatrix} b_n\mathbf{s_I} + \mathbf{w_I} \\ \mathbf{w_{LK-I}} \end{bmatrix}\begin{bmatrix} b_n\mathbf{s_I^T} + \mathbf{w_I^T} & \mathbf{w_{LK-I}^T} \end{bmatrix}\right] \\ &= \begin{bmatrix} \mathbf{S_I} + \mathbf{N_I} & \mathbf{0} \\ \mathbf{0} & \mathbf{N_{LK-I}} \end{bmatrix}, \end{aligned} \tag{4.23}$$

where

$$\mathbf{S_I} = E_p \begin{bmatrix} \alpha_1^2 R_g^2(\tilde{\tau}_1) & \alpha_1\alpha_2 R_g(\tilde{\tau}_1)R_g(\tilde{\tau}_2) & \cdots & \alpha_1\alpha_I R_g(\tilde{\tau}_1)R_g(\tilde{\tau}_I) \\ \alpha_2\alpha_1 R_g(\tilde{\tau}_2)R_g(\tilde{\tau}_1) & \alpha_2^2 R_g^2(\tilde{\tau}_2) & \cdots & \alpha_2\alpha_I R_g(\tilde{\tau}_2)R_g(\tilde{\tau}_I) \\ \vdots & \vdots & \ddots & \vdots \\ \alpha_I\alpha_1 R_g(\tilde{\tau}_I)R_g(\tilde{\tau}_1) & \alpha_I\alpha_2 R_g(\tilde{\tau}_I)R_g(\tilde{\tau}_2) & \cdots & \alpha_I^2 R_g^2(\tilde{\tau}_I) \end{bmatrix}, \tag{4.24}$$

$$\mathbf{N_I} = \frac{N_0}{2}\mathbf{I_{I\times I}}, \tag{4.25}$$

$$\mathbf{N_{LK-I}} = \frac{N_0}{2}\mathbf{I_{(LK-I)\times(LK-I)}}, \tag{4.26}$$

and $\mathbf{I_{P\times P}}$ denotes the $P\times P$ identity matrix. Therefore,

$$\left(E\left[\mathbf{v}\mathbf{v}^{\mathbf{T}}\right]\right)^{-1} = \begin{bmatrix} (\mathbf{S_I}+\mathbf{N_I})^{-1} & \mathbf{0} \\ \mathbf{0} & \mathbf{N_{LK-I}^{-1}} \end{bmatrix}. \tag{4.27}$$

The desired signal for the n^{th} data bit is given by:

$$d_n = \sqrt{E_p}\, b_n \int_0^{T_f} g^2(t)dt = \sqrt{E_p}\, b_n . \tag{4.28}$$

From (4.15) and (4.28),

$$E[d_n\mathbf{v}] = \sqrt{E_p}\, b_n E\begin{bmatrix} b_n\mathbf{s_I} + \mathbf{w_I} \\ \mathbf{w_{LK-I}} \end{bmatrix} = \sqrt{E_p}\begin{bmatrix} \mathbf{s_I} \\ \mathbf{0_{LK-I}} \end{bmatrix}, \tag{4.29}$$

where $\mathbf{0_{LK-I}}$ denotes the column vector with $L\times K - I$ zero elements.

Substitute (4.27) and (4.29) to (4.22):

$$\begin{aligned} \mathbf{c_o} &= \begin{bmatrix} (\mathbf{S_I}+\mathbf{N_I})^{-1} & \mathbf{0} \\ \mathbf{0} & \mathbf{N_{LK-I}^{-1}} \end{bmatrix} \cdot \sqrt{E_p}\begin{bmatrix} \mathbf{s_I} \\ \mathbf{0_{LK-I}} \end{bmatrix} \\ &= \sqrt{E_p}\begin{bmatrix} (\mathbf{S_I}+\mathbf{N_I})^{-1}\cdot\mathbf{s_I} \\ \mathbf{0} \end{bmatrix}. \end{aligned} \tag{4.30}$$

From (4.24), it is observed that $\mathbf{S_I}$ is a rank-1 symmetric matrix. Using eigenvalue decomposition [51], it can be written as:

$$\mathbf{S_I} = \mathbf{Q}\boldsymbol{\Lambda}_\mathbf{S}\mathbf{Q}^\mathbf{T}, \tag{4.31}$$

where

$$\mathbf{Q} = \frac{1}{\sqrt{\eta}}\begin{bmatrix} \alpha_1 R_g(\tilde{\tau}_1) & 0 & \cdots & 0 \\ \alpha_2 R_g(\tilde{\tau}_2) & 0 & \cdots & 0 \\ \vdots & \vdots & \ddots & \vdots \\ \alpha_I R_g(\tilde{\tau}_I) & 0 & \cdots & 0 \end{bmatrix}, \tag{4.32}$$

is the matrix containing all the eigenvectors of $\mathbf{S_I}$ and

$$\boldsymbol{\Lambda}_\mathbf{S} = \eta E_p \mathbf{I}_{\mathbf{I}\times\mathbf{I}}, \tag{4.33}$$

is a diagonal matrix with equivalent eigenvalues of $\mathbf{S_I}$:

$$\varsigma_i = \eta E_p,\ i = 1,2,\ldots I, \tag{4.34}$$

as the diagonal elements. Recall the matrix inversion lemma [52]:

$$(\mathbf{A}+\mathbf{BCD})^{-1} = \mathbf{A}^{-1} - \mathbf{A}^{-1}\mathbf{B}\left[\mathbf{C}^{-1} + \mathbf{D}\mathbf{A}^{-1}\mathbf{B}\right]^{-1}\mathbf{D}\mathbf{A}^{-1}, \tag{4.35}$$

and let $\mathbf{A} = \mathbf{N_I}$, $\mathbf{B} = \mathbf{Q}$, $\mathbf{C} = \boldsymbol{\Lambda}_\mathbf{S}$, $\mathbf{D} = \mathbf{Q}^\mathbf{T}$, then:

$$\begin{aligned}(\mathbf{S_I} + \mathbf{N_I})^{-1} &= (\mathbf{N_I} + \mathbf{Q}\boldsymbol{\Lambda}_\mathbf{S}\mathbf{Q}^\mathbf{T})^{-1} \\ &= \mathbf{N_I}^{-1} - \mathbf{N_I}^{-1}\mathbf{Q}\left[\boldsymbol{\Lambda}_\mathbf{S}^{-1} + \mathbf{Q}^\mathbf{T}\mathbf{N_I}^{-1}\mathbf{Q}\right]^{-1}\mathbf{Q}^\mathbf{T}\mathbf{N_I}^{-1}.\end{aligned} \tag{4.36}$$

Equations (4.37)-(4.39) below derive the expression for $(\mathbf{S_I} + \mathbf{N_I})^{-1}$ step by step:

$$\boldsymbol{\Lambda}_\mathbf{S}^{-1} + \mathbf{Q}^\mathbf{T}\mathbf{N_I}^{-1}\mathbf{Q}$$

$$= \frac{1}{\eta E_p}\mathbf{I}_{\mathbf{I}\times\mathbf{I}} + \frac{1}{\sqrt{\eta}}\begin{bmatrix} \alpha_1 R_g(\tilde{\tau}_1) & \alpha_2 R_g(\tilde{\tau}_2) & \cdots & \alpha_I R_g(\tilde{\tau}_I) \\ 0 & 0 & \cdots & 0 \\ \vdots & \vdots & \ddots & \vdots \\ 0 & 0 & \cdots & 0 \end{bmatrix}$$

$$\cdot \frac{2}{N_0}\mathbf{I}_{\mathbf{I}\times\mathbf{I}} \cdot \frac{1}{\sqrt{\eta}}\begin{bmatrix} \alpha_1 R_g(\tilde{\tau}_1) & 0 & \cdots & 0 \\ \alpha_2 R_g(\tilde{\tau}_2) & 0 & \cdots & 0 \\ \vdots & \vdots & \ddots & \vdots \\ \alpha_I R_g(\tilde{\tau}_I) & 0 & \cdots & 0 \end{bmatrix}$$

$$= \frac{1}{\eta E_p}\mathbf{I}_{\mathbf{I}\times\mathbf{I}} + \frac{2}{\eta N_0}\begin{bmatrix} \eta & 0 & \cdots & 0 \\ 0 & 0 & \cdots & 0 \\ \vdots & \vdots & \ddots & \vdots \\ 0 & 0 & \cdots & 0 \end{bmatrix}$$

$$= \begin{bmatrix} \frac{1}{\eta E_p} + \frac{2}{N_0} & 0 & \cdots & 0 \\ 0 & \frac{1}{\eta E_p} & \cdots & 0 \\ \vdots & \vdots & \ddots & \vdots \\ 0 & 0 & \cdots & \frac{1}{\eta E_p} \end{bmatrix}. \tag{4.37}$$

$$\Rightarrow \mathbf{Q}\left(\mathbf{\Lambda_S}^{-1} + \mathbf{Q^T}\mathbf{N_I}^{-1}\mathbf{Q}\right)^{-1}\mathbf{Q^T}$$

$$= \frac{1}{\sqrt{\eta}}\begin{bmatrix} \alpha_1 R_g(\tilde{\tau}_1) & 0 & \cdots & 0 \\ \alpha_2 R_g(\tilde{\tau}_2) & 0 & \cdots & 0 \\ \vdots & \vdots & \ddots & \vdots \\ \alpha_I R_g(\tilde{\tau}_I) & 0 & \cdots & 0 \end{bmatrix} \cdot \begin{bmatrix} \frac{1}{\eta E_p} + \frac{2}{N_0} & 0 & \cdots & 0 \\ 0 & \frac{1}{\eta E_p} & \cdots & 0 \\ \vdots & \vdots & \ddots & \vdots \\ 0 & 0 & \cdots & \frac{1}{\eta E_p} \end{bmatrix}^{-1}$$

$$\cdot \frac{1}{\sqrt{\eta}}\begin{bmatrix} \alpha_1 R_g(\tilde{\tau}_1) & \alpha_2 R_g(\tilde{\tau}_2) & \cdots & \alpha_I R_g(\tilde{\tau}_I) \\ 0 & 0 & \cdots & 0 \\ \vdots & \vdots & \ddots & \vdots \\ 0 & 0 & \cdots & 0 \end{bmatrix}$$

$$= \frac{1}{\eta}\left(\frac{1}{\eta E_p} + \frac{2}{N_0}\right)^{-1}\begin{bmatrix} \alpha_1 R_g(\tilde{\tau}_1) & 0 & \cdots & 0 \\ \alpha_2 R_g(\tilde{\tau}_2) & 0 & \cdots & 0 \\ \vdots & \vdots & \ddots & \vdots \\ \alpha_I R_g(\tilde{\tau}_I) & 0 & \cdots & 0 \end{bmatrix}\begin{bmatrix} \alpha_1 R_g(\tilde{\tau}_1) & \alpha_2 R_g(\tilde{\tau}_2) & \cdots & \alpha_I R_g(\tilde{\tau}_I) \\ 0 & 0 & \cdots & 0 \\ \vdots & \vdots & \ddots & \vdots \\ 0 & 0 & \cdots & 0 \end{bmatrix}$$

$$= \frac{N_0 E_p}{N_0 + 2\eta E_p} \begin{bmatrix} \alpha_1^2 R_g^2(\tilde{\tau}_1) & \alpha_1\alpha_2 R_g(\tilde{\tau}_1) R_g(\tilde{\tau}_2) & \cdots & \alpha_1\alpha_I R_g(\tilde{\tau}_1) R_g(\tilde{\tau}_I) \\ \alpha_2\alpha_1 R_g(\tilde{\tau}_2) R_g(\tilde{\tau}_1) & \alpha_2^2 R_g^2(\tilde{\tau}_2) & \cdots & \alpha_2\alpha_I R_g(\tilde{\tau}_2) R_g(\tilde{\tau}_I) \\ \vdots & \vdots & \ddots & \vdots \\ \alpha_I\alpha_1 R_g(\tilde{\tau}_I) R_g(\tilde{\tau}_1) & \alpha_I\alpha_2 R_g(\tilde{\tau}_I) R_g(\tilde{\tau}_2) & \cdots & \alpha_I^2 R_g^2(\tilde{\tau}_I) \end{bmatrix}. \quad (4.38)$$

Substitute (4.25) and (4.38) back to (4.36):

$$(\mathbf{S_I} + \mathbf{N_I})^{-1}$$

$$= \frac{2}{N_0}\mathbf{I_{I\times I}} - \frac{2}{N_0}\mathbf{I_{I\times I}} \frac{N_0 E_p}{N_0 + 2\eta E_p}$$

$$\cdot \begin{bmatrix} \alpha_1^2 R_g^2(\tilde{\tau}_1) & \alpha_1\alpha_2 R_g(\tilde{\tau}_1) R_g(\tilde{\tau}_2) & \cdots & \alpha_1\alpha_I R_g(\tilde{\tau}_1) R_g(\tilde{\tau}_I) \\ \alpha_2\alpha_1 R_g(\tilde{\tau}_2) R_g(\tilde{\tau}_1) & \alpha_2^2 R_g^2(\tilde{\tau}_2) & \cdots & \alpha_2\alpha_I R_g(\tilde{\tau}_2) R_g(\tilde{\tau}_I) \\ \vdots & \vdots & \ddots & \vdots \\ \alpha_I\alpha_1 R_g(\tilde{\tau}_I) R_g(\tilde{\tau}_1) & \alpha_I\alpha_2 R_g(\tilde{\tau}_I) R_g(\tilde{\tau}_2) & \cdots & \alpha_I^2 R_g^2(\tilde{\tau}_I) \end{bmatrix} \cdot \frac{2}{N_0}\mathbf{I_{I\times I}}$$

$$= \frac{2}{N_0}\mathbf{I_{I\times I}} - \frac{4E_p}{N_0(N_0 + 2\eta E_p)}$$

$$\cdot \begin{bmatrix} \alpha_1^2 R_g^2(\tilde{\tau}_1) & \alpha_1\alpha_2 R_g(\tilde{\tau}_1) R_g(\tilde{\tau}_2) & \cdots & \alpha_1\alpha_I R_g(\tilde{\tau}_1) R_g(\tilde{\tau}_I) \\ \alpha_2\alpha_1 R_g(\tilde{\tau}_2) R_g(\tilde{\tau}_1) & \alpha_2^2 R_g^2(\tilde{\tau}_2) & \cdots & \alpha_2\alpha_I R_g(\tilde{\tau}_2) R_g(\tilde{\tau}_I) \\ \vdots & \vdots & \ddots & \vdots \\ \alpha_I\alpha_1 R_g(\tilde{\tau}_I) R_g(\tilde{\tau}_1) & \alpha_I\alpha_2 R_g(\tilde{\tau}_I) R_g(\tilde{\tau}_2) & \cdots & \alpha_I^2 R_g^2(\tilde{\tau}_I) \end{bmatrix}$$

$$= \frac{2}{N_0}\mathbf{I_{I\times I}} - \frac{4}{N_0(N_0 + 2\eta E_p)}\mathbf{S_I}. \quad (4.39)$$

To obtain the optimum value of tap weight from (4.30),

$$\sqrt{E_p}(\mathbf{S_I} + \mathbf{N_I})^{-1} \cdot \mathbf{s_I}$$

$$= \sqrt{E_p}\left(\frac{2}{N_0}\mathbf{I_{I\times I}} - \frac{4}{N_0(N_0 + 2\eta E_p)}\mathbf{S_I}\right)\sqrt{E_p}\begin{bmatrix} \alpha_1 R_g(\tilde{\tau}_1) \\ \alpha_2 R_g(\tilde{\tau}_2) \\ \vdots \\ \alpha_I R_g(\tilde{\tau}_I) \end{bmatrix}$$

$$= \frac{2E_p}{N_0}\begin{bmatrix} \alpha_1 R_g(\tilde{\tau}_1) \\ \alpha_2 R_g(\tilde{\tau}_2) \\ \vdots \\ \alpha_I R_g(\tilde{\tau}_I) \end{bmatrix} - \frac{4E_p^2}{N_0\left(N_0 + 2\eta E_p\right)}$$

$$\cdot \begin{bmatrix} \alpha_1^2 R_g^2(\tilde{\tau}_1) & \alpha_1\alpha_2 R_g(\tilde{\tau}_1)R_g(\tilde{\tau}_2) & \cdots & \alpha_1\alpha_I R_g(\tilde{\tau}_1)R_g(\tilde{\tau}_I) \\ \alpha_2\alpha_1 R_g(\tilde{\tau}_2)R_g(\tilde{\tau}_1) & \alpha_2^2 R_g^2(\tilde{\tau}_2) & \cdots & \alpha_2\alpha_I R_g(\tilde{\tau}_2)R_g(\tilde{\tau}_I) \\ \vdots & \vdots & \ddots & \vdots \\ \alpha_I\alpha_1 R_g(\tilde{\tau}_I)R_g(\tilde{\tau}_1) & \alpha_I\alpha_2 R_g(\tilde{\tau}_I)R_g(\tilde{\tau}_2) & \cdots & \alpha_I^2 R_g^2(\tilde{\tau}_I) \end{bmatrix} \cdot \begin{bmatrix} \alpha_1 R_g(\tilde{\tau}_1) \\ \alpha_2 R_g(\tilde{\tau}_2) \\ \vdots \\ \alpha_I R_g(\tilde{\tau}_I) \end{bmatrix}$$

$$= \frac{2E_p}{N_0}\begin{bmatrix} \alpha_1 R_g(\tilde{\tau}_1) \\ \alpha_2 R_g(\tilde{\tau}_2) \\ \vdots \\ \alpha_I R_g(\tilde{\tau}_I) \end{bmatrix} - \frac{4E_p^2\left(\alpha_1^2 R_g^2(\tilde{\tau}_1) + \alpha_2^2 R_g^2(\tilde{\tau}_2) + \cdots + \alpha_I^2 R_g^2(\tilde{\tau}_I)\right)}{N_0\left(N_0 + 2\eta E_p\right)}\begin{bmatrix} \alpha_1 R_g(\tilde{\tau}_1) \\ \alpha_2 R_g(\tilde{\tau}_2) \\ \vdots \\ \alpha_I R_g(\tilde{\tau}_I) \end{bmatrix}$$

$$= \left(\frac{2E_p}{N_0} - \frac{4\eta E_p^2}{N_0\left(N_0 + 2\eta E_p\right)}\right)\begin{bmatrix} \alpha_1 R_g(\tilde{\tau}_1) \\ \alpha_2 R_g(\tilde{\tau}_2) \\ \vdots \\ \alpha_I R_g(\tilde{\tau}_I) \end{bmatrix}$$

$$= \frac{2E_p N_0}{N_0\left(N_0 + 2\eta E_p\right)}\begin{bmatrix} \alpha_1 R_g(\tilde{\tau}_1) \\ \alpha_2 R_g(\tilde{\tau}_2) \\ \vdots \\ \alpha_I R_g(\tilde{\tau}_I) \end{bmatrix}$$

$$= \frac{1}{\frac{1}{\gamma} + \eta}\begin{bmatrix} \alpha_1 R_g(\tilde{\tau}_1) \\ \alpha_2 R_g(\tilde{\tau}_2) \\ \vdots \\ \alpha_I R_g(\tilde{\tau}_I) \end{bmatrix}, \tag{4.40}$$

where γ is the input SNR defined as:

$$\gamma = \frac{E_p}{\frac{N_0}{2}}, \tag{4.41}$$

Comparing (4.30) and (4.40), the optimum tap weights can be obtained as:

$$c_i^o = \begin{cases} \dfrac{\alpha_i R_g(\tilde{\tau}_i)}{\dfrac{1}{\gamma} + \eta} & i = 1,2,\ldots,I \\ 0 & i = I+1, I+2,\ldots,L\times K \end{cases}. \tag{4.42}$$

4.3 LMS Analysis

The optimum tap weights obtained in Section 4.2 are derived using Wiener solution. In practical implementations, the tap weights are adapted recursively using LMS technique. Thus there is an additional error term associated with the adaptation step size μ for each tap weight as follows:

$$c_i^{LMS} = c_i^o + e_i^{LMS}, \tag{4.43}$$

where the variance of the error is given by [53]:

$$\sigma_{e_i}^2 = \sigma_{e_i^{LMS}}^2 = \frac{\mu J_{\min}}{2 - \mu\lambda_i}, \tag{4.44}$$

when the tap value converges. The mean value of the error is zero when the tap value converges. Here $J_{\min}$ is the minimum value of the cost function (4.21) when the optimum Wiener solution is achieved [53]:

$$J_{\min} = d_n^2 - \mathbf{c_o^T} E\left[\mathbf{v}\mathbf{v}^T\right]\mathbf{c_o}, \tag{4.45}$$

and λ_i is the eigenvalue associated with the autocorrelation matrix of the input data given by (4.23). From (4.23), (4.25), (4.26), (4.31) and (4.33), the eigenvalue of (4.23) can be derived as:

$$\lambda_i = \begin{cases} \eta E_p + \dfrac{N_0}{2} & i = 1,2,\ldots,I \\ \dfrac{N_0}{2} & i = I+1, I+2,\ldots, L\times K \end{cases}. \tag{4.46}$$

By substituting (4.23), (4.28), (4.30) and (4.40) into (4.45), the minimum value of the cost function can be calculated as:

$$J_{\min} = \left(\sqrt{E_p} b_n\right)^2 - \sqrt{E_p}\begin{bmatrix} (\mathbf{S_I} + \mathbf{N_I})^{-1} \cdot \mathbf{s_I} \\ \mathbf{0} \end{bmatrix}^T \cdot \begin{bmatrix} \mathbf{S_I} + \mathbf{N_I} & \mathbf{0} \\ \mathbf{0} & \mathbf{N_{LK-I}} \end{bmatrix} \cdot \sqrt{E_p}\begin{bmatrix} (\mathbf{S_I} + \mathbf{N_I})^{-1} \cdot \mathbf{s_I} \\ \mathbf{0} \end{bmatrix}.$$

$$= E_p - E_p \begin{bmatrix} \mathbf{s_I^T} & \mathbf{0} \end{bmatrix} \cdot \begin{bmatrix} (\mathbf{S_I} + \mathbf{N_I})^{-1} \cdot \mathbf{s_I} \\ \mathbf{0} \end{bmatrix}$$

$$= E_p - E_p \cdot \sqrt{E_p}\left[\alpha_1 R_g(\tilde{\tau}_1) \;\; \alpha_2 R_g(\tilde{\tau}_2) \;\; \ldots \;\; \alpha_I R_g(\tilde{\tau}_I) \; 0 \; \ldots \; 0 \;\; 0\right] \cdot \frac{2\sqrt{E_p}}{N_0 + 2\eta E_p}$$
$$\cdot \left[\alpha_1 R_g(\tilde{\tau}_1) \;\; \alpha_2 R_g(\tilde{\tau}_2) \;\; \ldots \;\; \alpha_I R_g(\tilde{\tau}_I) \; 0 \; \ldots \; 0 \;\; 0\right]^T$$

$$= E_p - \frac{2\eta E_p^2}{N_0 + 2\eta E_p}$$

$$= \frac{E_p}{1 + \eta\gamma}. \tag{4.47}$$

From (4.44), (4.46) and (4.47), the variance of the LMS error term, for $i = 1,2,\ldots,I$, can be expressed as:

$$\sigma_{e_i}^2 = \frac{\mu J_{\min}}{2 - \mu\lambda_i} = \frac{\mu E_p}{(1 + \eta\gamma)\left(2 - \mu\left(\eta E_p + \frac{N_0}{2}\right)\right)}. \tag{4.48}$$

Similarly, for $i = I+1, I+2,\ldots, L\times K$, the LMS error term is:

$$\sigma_{e_i}^2 = \frac{\mu J_{\min}}{2-\mu\lambda_i} = \frac{\mu E_p}{(1+\eta\gamma)\left(2-\mu\frac{N_0}{2}\right)}. \tag{4.49}$$

The decision signal, y_n, as shown in (4.19), can be expressed as the sum of two terms:

$$y_n = \mathbf{c}^{\mathbf{T}}\mathbf{v} = \sum_{i=1}^{LK} c_i^{LMS} v_i = \sum_{i=1}^{I} c_i^{LMS} v_i + \sum_{i=I+1}^{LK} c_i^{LMS} v_i \ . \tag{4.50}$$

From (4.15), (4.42), and (4.43),

$$\sum_{i=1}^{I} c_i^{LMS} v_i = \sum_{i=1}^{I} \left(\left(\frac{\alpha_i R_g(\tilde{\tau}_i)}{\frac{1}{\gamma}+\eta} + e_i^{LMS} \right) \cdot \left(b_n \sqrt{E_p}\, \alpha_i R_g(\tilde{\tau}_i) + w_i \right) \right)$$

$$= \frac{b_n \sqrt{E_p}}{\frac{1}{\gamma}+\eta} \sum_{i=1}^{I} \alpha_i^2 R_g^2(\tilde{\tau}_i) + \sum_{i=1}^{I} e_i^{LMS} w_i + \frac{1}{\frac{1}{\gamma}+\eta} \sum_{i=1}^{I} \alpha_i R_g(\tilde{\tau}_i) w_i + b_n \sqrt{E_p} \sum_{i=1}^{I} e_i^{LMS} \alpha_i R_g(\tilde{\tau}_i). \tag{4.51}$$

Similarly, it can be shown:

$$\sum_{i=I+1}^{LK} c_i^{LMS} v_i = \sum_{i=I+1}^{LK} (0 + e_i^{LMS}) w_i = \sum_{i=I+1}^{LK} e_i^{LMS} w_i \ . \tag{4.52}$$

Substituting (4.51) and (4.52) back to (4.50), the decision signal is shown to be:

$$y_n = \sum_{i=1}^{I} c_i^{LMS} v_i + \sum_{i=I+1}^{LK} c_i^{LMS} v_i$$

$$= \frac{b_n \sqrt{E_p}}{\frac{1}{\gamma}+\eta} \sum_{i=1}^{I} \alpha_i^2 R_g^2(\tilde{\tau}_i) + \sum_{i=1}^{I} e_i^{LMS} w_i + \frac{1}{\frac{1}{\gamma}+\eta} \sum_{i=1}^{I} \alpha_i R_g(\tilde{\tau}_i) w_i + b_n \sqrt{E_p} \sum_{i=1}^{I} e_i^{LMS} \alpha_i R_g(\tilde{\tau}_i) + \sum_{i=I+1}^{LK} e_i^{LMS} w_i$$

$$= \frac{b_n \eta \sqrt{E_p}}{\frac{1}{\gamma} + \eta} + \frac{1}{\frac{1}{\gamma} + \eta} \sum_{i=1}^{I} \alpha_i R_g(\tilde{\tau}_i) w_i + b_n \sqrt{E_p} \sum_{i=1}^{I} e_i^{LMS} \alpha_i R_g(\tilde{\tau}_i) + \sum_{i=1}^{LK} e_i^{LMS} w_i \,. \quad (4.53)$$

The first term in the above equation represents the signal portion, while the rest three terms are the noise induced by the channel as well as LMS adaptation process.

4.4 BER Expression

The performance of the proposed receiver is evaluated by the BER it can achieve. From (2.8), the BER is determined by the receiver output SNR.

Referring to (4.53), the output SNR can be obtained by taking the ratio of the signal power over the expected noise power in the decision signal:

$$SNR_o = \frac{\left(\frac{b_n \eta \sqrt{E_p}}{\frac{1}{\gamma} + \eta} \right)^2}{E\left[\left(\frac{1}{\frac{1}{\gamma} + \eta} \sum_{i=1}^{I} \alpha_i R_g(\tilde{\tau}_i) w_i + b_n \sqrt{E_p} \sum_{i=1}^{I} e_i^{LMS} \alpha_i R_g(\tilde{\tau}_i) + \sum_{i=1}^{LK} e_i^{LMS} w_i \right)^2 \right]}. \quad (4.54)$$

Assume the LMS error is uncorrelated with the noise [51], i.e.,

$$E\left[e_i^{LMS} w_j\right] = E\left[e_i^{LMS}\right] \cdot E\left[w_j\right], \forall i = 1,2,\ldots L \times K,\ j = 1,2,\ldots L \times K. \quad (4.55)$$

Then the denominator of (4.54) is simply the sum of the expectations of the three individual square terms, since the noise and LMS error both have zero mean. The three expected square terms are evaluated one by one in the following.

$$E\left[\left(\frac{1}{\frac{1}{\gamma} + \eta} \sum_{i=1}^{I} \alpha_i R_g(\tilde{\tau}_i) w_i \right)^2 \right] = \frac{E\left[\left(\sum_{i=1}^{I} \alpha_i R_g(\tilde{\tau}_i) w_i \right)^2 \right]}{\left(\frac{1}{\gamma} + \eta \right)^2}$$

$$= \frac{\sum_{i=1}^{I} \alpha_i^2 R_g^2(\tilde{\tau}_i) E\left[w_i^2\right]}{\left(\frac{1}{\gamma} + \eta\right)^2} = \frac{\eta \sigma_{w_i}^2}{\left(\frac{1}{\gamma} + \eta\right)^2}$$

$$= \frac{\eta N_0}{2\left(\frac{1}{\gamma} + \eta\right)^2}. \tag{4.56}$$

$$E\left[\left(b_n \sqrt{E_p} \sum_{i=1}^{I} e_i^{LMS} \alpha_i R_g(\tilde{\tau}_i)\right)^2\right] = E_p \cdot E\left[\sum_{i=1}^{I} \alpha_i^2 R_g^2(\tilde{\tau}_i) \sigma_{e_i}^2\right]. \tag{4.57}$$

Substitute (4.48) into (4.57):

$$E\left[\left(b_n \sqrt{E_p} \sum_{i=1}^{I} e_i^{LMS} \alpha_i R_g(\tilde{\tau}_i)\right)^2\right] = \frac{\mu \eta E_p^2}{(1+\eta\gamma)\left(2 - \mu\left(\eta E_p + \frac{N_0}{2}\right)\right)}. \tag{4.58}$$

$$E\left[\left(\sum_{i=1}^{LK} e_i^{LMS} w_i\right)^2\right] = \sum_{i=1}^{LK} \left(E\left[\left(e_i^{LMS}\right)^2\right] \cdot E\left[\left(w_i^2\right)\right]\right) = \sum_{i=1}^{LK} \sigma_{e_i}^2 \sigma_{w_i}^2 = \sigma_{w_i}^2 \left(\sum_{i=1}^{I} \sigma_{e_i}^2 + \sum_{i=I+1}^{LK} \sigma_{e_i}^2\right). \tag{4.59}$$

Substituting (4.48) and (4.49) into (4.59), it can be shown:

$$E\left[\left(\sum_{i=1}^{LK} e_i^{LMS} w_i\right)^2\right] = \frac{N_0}{2}\left(\frac{\mu I E_p}{(1+\eta\gamma)\left(2 - \mu\left(\eta E_p + \frac{N_0}{2}\right)\right)} + \frac{\mu(LK - I)E_p}{(1+\eta\gamma)\left(2 - \mu\frac{N_0}{2}\right)}\right). \tag{4.60}$$

The denominator of (4.54) is the sum of (4.56), (4.58) and (4.60):

$$E\left[\left(\frac{1}{\frac{1}{\gamma}+\eta}\sum_{i=1}^{I}\alpha_i R_g(\tilde{\tau}_i)w_i + b_n\sqrt{E_p}\sum_{i=1}^{I}e_i^{LMS}\alpha_i R_g(\tilde{\tau}_i) + \sum_{i=1}^{LK}e_i^{LMS}w_i\right)^2\right]$$

$$= \frac{\eta N_0}{2\left(\frac{1}{\gamma}+\eta\right)^2} + \frac{\mu\eta E_p^2}{(1+\eta\gamma)\left(2-\mu\left(\eta E_p+\frac{N_0}{2}\right)\right)}$$

$$+ \frac{N_0}{2}\left(\frac{\mu I E_p}{(1+\eta\gamma)\left(2-\mu\left(\eta E_p+\frac{N_0}{2}\right)\right)} + \frac{\mu(LK-I)E_p}{(1+\eta\gamma)\left(2-\mu\frac{N_0}{2}\right)}\right)$$

$$= \frac{N_0\gamma\left(\mu E_p\left(\frac{1}{\gamma}+\eta\right)\left(\frac{I+\eta\gamma}{2\gamma^2-\mu\gamma E_p(1+\eta\gamma)}+\frac{LK-I}{2\gamma^2-\mu\gamma E_p}\right)+\frac{\eta}{\gamma}\right)}{2\left(\frac{1}{\gamma}+\eta\right)^2}. \quad (4.61)$$

Substitute (4.61) to (4.54), the output SNR can be expressed as:

$$SNR_o = \frac{\frac{\eta^2 E_p}{\left(\frac{1}{\gamma}+\eta\right)^2}}{\frac{N_0\gamma\left(\mu E_p\left(\frac{1}{\gamma}+\eta\right)\left(\frac{I+\eta\gamma}{2\gamma^2-\mu\gamma E_p(1+\eta\gamma)}+\frac{LK-I}{2\gamma^2-\mu\gamma E_p}\right)+\frac{\eta}{\gamma}\right)}{2\left(\frac{1}{\gamma}+\eta\right)^2}}$$

$$= \frac{\eta^2}{\mu E_p\left(\frac{1}{\gamma}+\eta\right)\left(\frac{I+\eta\gamma}{2\gamma^2-\mu\gamma E_p(1+\eta\gamma)}+\frac{LK-I}{2\gamma^2-\mu\gamma E_p}\right)+\frac{\eta}{\gamma}}. \quad (4.62)$$

If the step size μ is very small and approaches to 0, the first term in the denominator of (4.62) can be ignored and the SNR term is much simplified:

$$SNR_o \approx \frac{\eta^2}{\frac{\eta}{\gamma}} = \eta\gamma . \tag{4.63}$$

Therefore the BER can be easily obtained from the output SNR as (2.8):

$$P_b = Q\left(\sqrt{SNR_o}\right) = Q\left(\sqrt{\eta\gamma}\right). \tag{4.64}$$

4.5 Misadjustment

The misadjustment of the cost function due to the LMS adaptation is given by [51]:

$$\mathcal{M} = \frac{J_{ex}(\infty)}{J_{\min}} = \frac{\mu}{2} tr\left(E\left[\mathbf{v}\mathbf{v}^{\mathbf{T}}\right]\right), \tag{4.65}$$

where $tr(\cdot)$ denotes the trace operation on the matrix and $J_{ex}(\infty)$ represents the excess MSE.

From (4.23), (4.24)-(4.26),

$$tr\left(E\left[\mathbf{v}\mathbf{v}^{\mathbf{T}}\right]\right) = tr(\mathbf{S_I}) + tr(\mathbf{N_I}) + tr(\mathbf{N_{LK-I}})$$

$$= E_p \sum_{i=1}^{I} \alpha_i^2 R_g^2(\tilde{\tau}_i) + I \cdot \frac{N_0}{2} + (LK - I) \cdot \frac{N_0}{2}$$

$$= E_p \eta + \frac{LKN_0}{2}. \tag{4.66}$$

Substituting (4.66) into (4.65), the upper bound of the misadjustment can be shown to be:

$$\mathcal{M} = \frac{\mu}{2}\left(E_p \eta + \frac{LKN_0}{2}\right) \le \frac{\mu E_p}{2}\left(1 + \frac{LK}{\gamma}\right). \tag{4.67}$$

In low power applications (small E_p), the misadjustment can be controlled to be very small with small enough adaptation step size μ.

5 SIMULATION RESULTS

In this chapter, extensive simulations are carried out to verify the theoretical results derived in chapter 4 as well as to compare the performance of the proposed BRake with other regular Rake structures. The simulation setup is as follows: the 2nd order derivative Gaussian monocycle as in (2.3) and channel models CM1-CM4 as in IEEE 802.15.3a [14] are employed. BPSK modulation is adopted with the transmission rate at 100MHz. The pulse width should be narrow enough to minimize the ISI and fit into the FCC spectrum, while pulses with too narrow width are difficult to generate in implementation and require extremely high sampling rate. Considering the tradeoff, the pulse width is set to 0.25 ns. Therefore the bandwidth of UWB signal is approximately 4 GHz. As this is an impulse radio scheme where no carrier is used, the operating frequency band would be 0 to 4 GHz. The emission power can be adjusted to meet the FCC frequency mask. 100 Monte Carlo realizations with 100,000 pulses in each trial are used for the BER calculation.

For CM1-CM2, 5 Rake branches are used with 8 taps in each branch as we have found this setting can achieve competitive performance to other Rake structures and the improvement is not significant by adding more branches or taps. Referring to section 3.3 and equations (3.8) and (3.9), the sampling rates for every branch are set to 0.5 ns, 0.65 ns, 0.85 ns, 1.1 ns and 1.4 ns, respectively; $\Delta\tau$ is set to be 0.65 ns. For CM3-CM4, 6 Rake branches are used with 8 taps in each branch since these two channels have more multipath components than CM1-CM2.

5.1 Theoretical versus Simulated BER

LMS algorithm is used for tap estimation. Figure 5.1 captures the weight (in absolute value) for every tap after algorithm converges in CM1 when SNR is 25 dB. It is not easy to find out the threshold value to discard the mis-sampled taps in this graph alone. In order to clearly obtain the proper threshold, some techniques are employed as follows. Firstly the 1st order derivative of the tab weight is calculated and plotted in Figure 5.2 (a). Then these data are up-sampled by a factor of 40 since the original data pool is too small (contains only 39 data) for its distribution pattern to be found. Next the histogram of the up-sampled data set is plotted in Figure 5.2 (b). It can be easily seen from Figure 5.2 (b) that the cut-off point should be set at 0.02. Back to Figure 5.2 (a), the threshold value 0.02 corresponds to tap 10. The difference of tap value after tap 10 are very small, and it can be seen from Figure 5.1 that the tap weights after tap 10 (tap 11 to tap 40) are very small, which means the successfully captured energy ratio was around 10/40 = 0.25. So η for CM1 in the theoretical BER calculation was set to 0.25. Based on this estimation of η, the theoretical BER performance curve is plotted according to (4.64), which matched very well to the simulated BER curve, as shown in Figure 5.3.

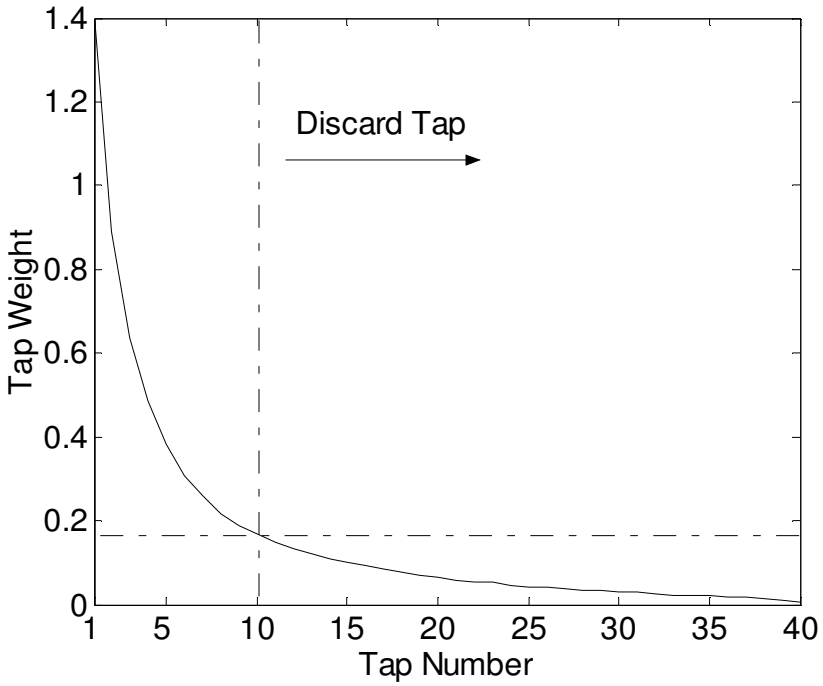

Figure 5.1 Tap weight.

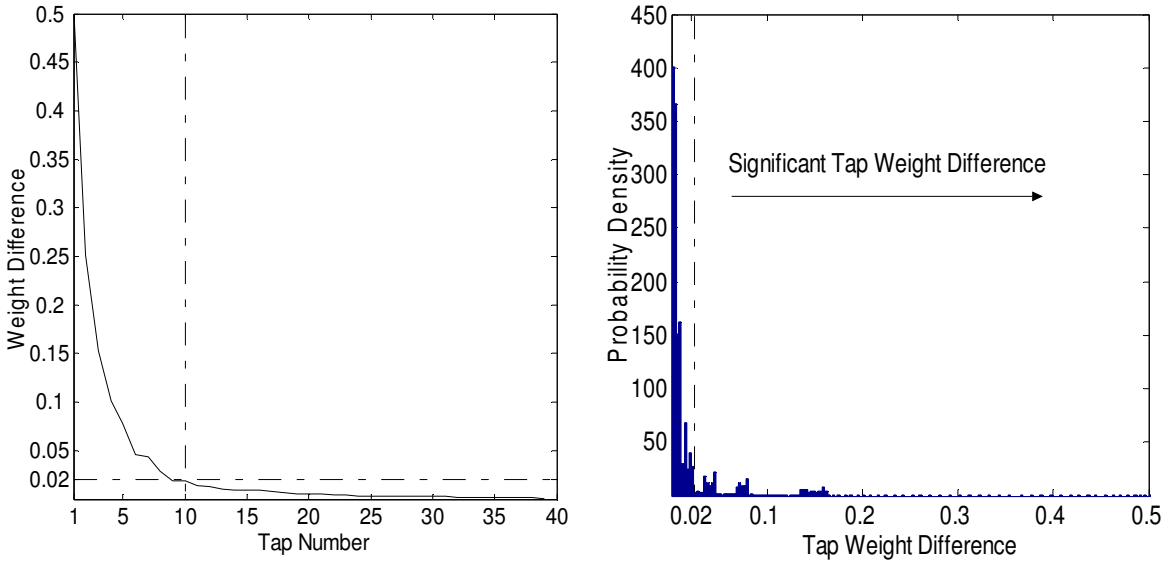

(a) Tap weight difference. (b) Histogram after upsampling.

Figure 5.2 Tap weight difference and its histogram.

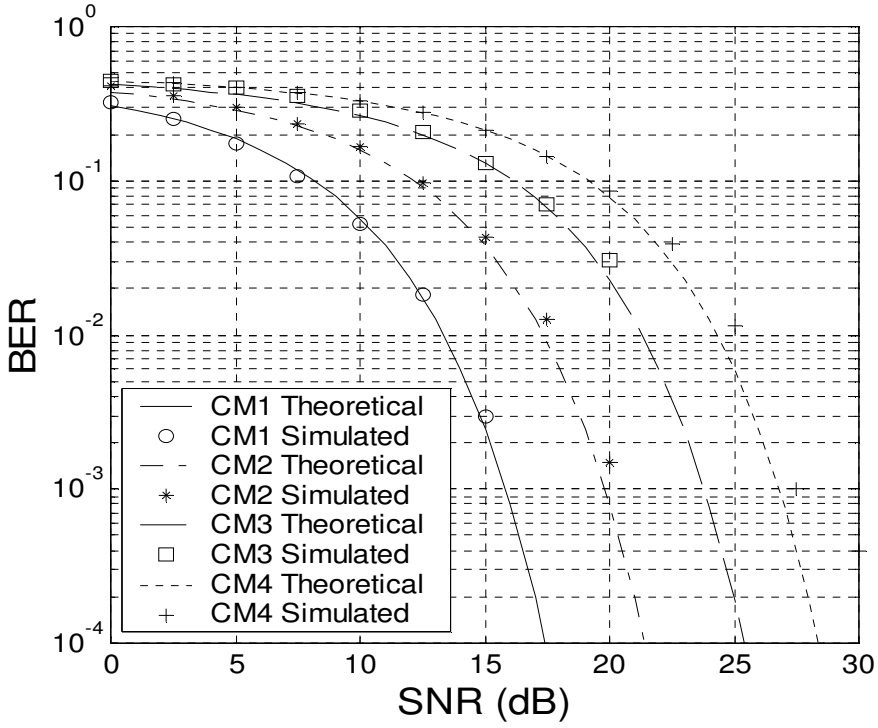

Figure 5.3 Theoretical versus simulated BER for CM1-CM4.

The curves for CM2-CM4 in Figure 5.3 are obtained in the same manner. In practice, there is no need to include all the taps in the BRake combing. After initial adaptation and estimation by training data set, proper threshold is obtained and small-value-taps are discarded. Therefore the receiver complexity can be further simplified. In this simulation, the initial set-up was 40 fingers for CM1-CM2 and 48 fingers for CM3-CM4. After tap convergence, the remaining useful fingers were less than 10, therefore greatly simplified the receiver complexity.

5.2 Effect of μ on BER Approximation

In section 4.4, the SNR expression is much simplified from (4.62) to (4.63) when we assume the step size μ is very small, i.e., it is assumed:

$$F = \mu E_p \left(\frac{1}{\gamma} + \eta \right) \left(\frac{I + \eta\gamma}{2\gamma^2 - \mu\gamma E_p (1 + \eta\gamma)} + \frac{LK - I}{2\gamma^2 - \mu\gamma E_p} \right) \approx 0 , \tag{5.1}$$

with small enough μ. This section examines the effect of μ on the validity of the approximation. In this simulation η, I, L and K were set to 0.25, 10, 5 and 8, respectively, which are consistent with the previous section .

To ensure the stability of the LMS algorithm, the step size μ is bounded by $0 < \mu < \frac{1}{3tr(\mathbf{R})}$ [51] where $\mathbf{R}$ is the autocorrelation matrix given by (4.23). From (4.66), the trace of the matrix is also associated with the power of input signal and input SNR. For a fixed pulse energy E_p, the smaller the input SNR, the bigger the noise power, and the bigger the trace. So μ should be upper bounded by the smallest input SNR which is 0 dB in our simulation. It is also found from (5.1) that F is proportionally related with E_p. However bigger E_p results in bigger $tr(\mathbf{R})$ and smaller upper bound of μ, therefore smaller F. To prove this, two simulations were carried out with E_p set to 3 and 300, respectively. The BER is obtained using (2.8) and (4.62). When $E_p = 3$, it is calculated that $\mu_{\max} = 2.6 \times 10^{-3}$. It can be seen from Figure 5.4 (a) that when μ is less than 2.6×10^{-3}, the BER performance is almost not affected by the variation of μ. In other

words it is reasonable to discard F, the first term of the denominator in (4.62), if $\mu < 2.6\times10^{-3}$. When $E_p = 300$, it can be calculated that $\mu_{\max} = 2.6\times10^{-5}$. The simulation results is shown in Figure 5.4 (b) and the same argument applies. Therefore the approximation from (4.62) to (4.63) is very appropriate.

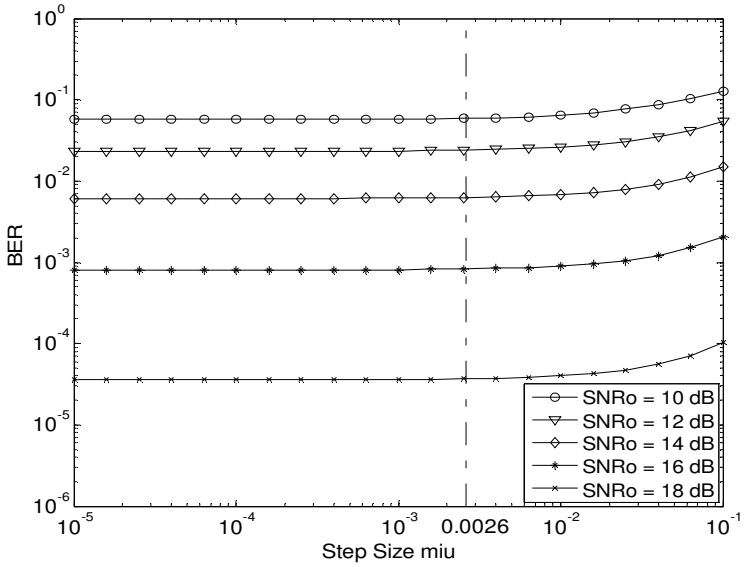

(a) BER approximation when $E_p = 3$.

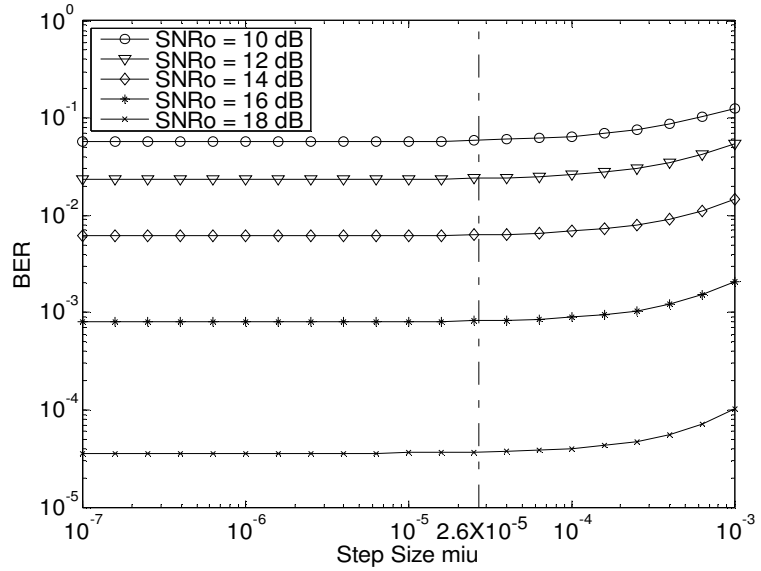

(b) BER approximation when $E_p = 300$.

Figure 5.4 Effect of μ on BER approximation.

5.3 BER Comparison with Other Rake Structures

The BER performance of BRake and conventional ARake, and SRake with 5 and 10 fingers of CM1-CM4 are shown in Figure 5.5 to Figure 5.8. It is seen that the BRake achieves satisfactory performance (with less than 5dB degradation for CM1-CM2 and less than 10dB degradation for CM3-CM4 from ARake, respectively) without employing channel estimation. Note the sampling rate for each branch of BRake is at sub-Nyquist signaling rate. In our setup, the pulse duration is 0.25 ns and the sampling rate for the first branch is 0.5 ns, which is at one quarter of the Nyquist rate (0.125 ns). Sampling rates for subsequent branches are even less as there are less energy we can collect at large delay times. This greatly relaxes the ADC requirements and significantly reduces the power consumption of the receiver in practical implementations.

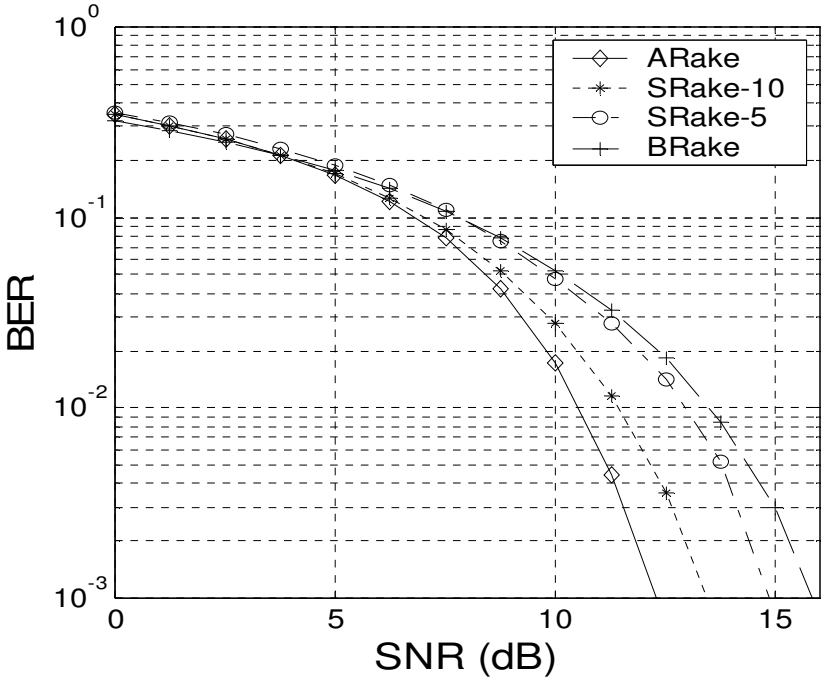

Figure 5.5 BER performance for CM1.

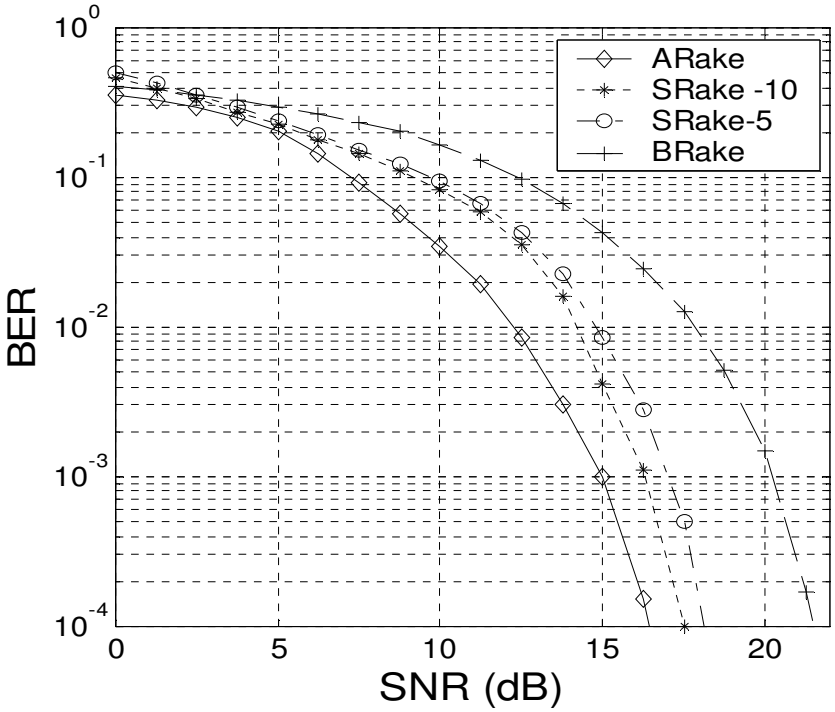

Figure 5.6 BER performance for CM2.

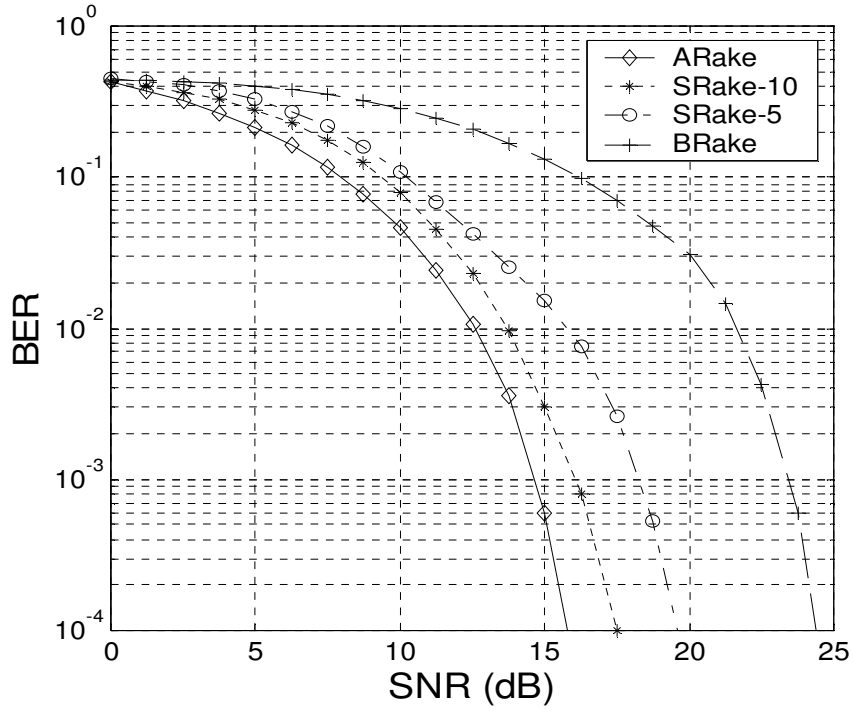

Figure 5.7 BER performance for CM3.

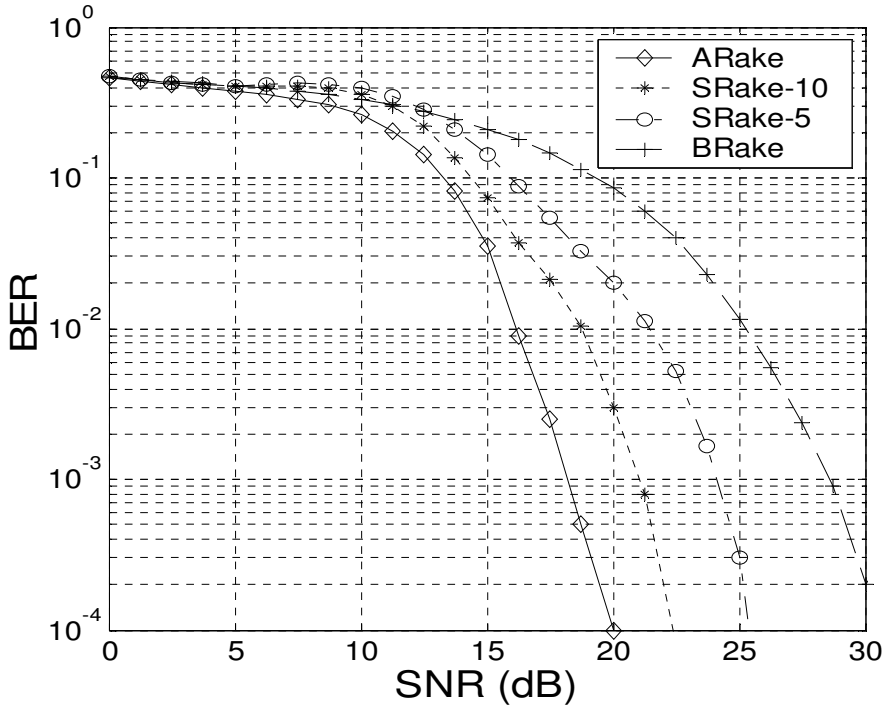

Figure 5.8 BER performance for CM4.

6 CONCLUSION

6.1 Conclusion Remarks

In this thesis a novel BRake receiver structure is proposed for UWB transmission systems. The performance analysis of the proposed algorithm has been carried out with closed form BER expression followed by simulations which prove the validity of the theoretical analysis and the feasibility of the implementation.

The first two chapters give a brief introduction of UWB history and design considerations. Two main UWB transmission schemes, IR and OFDM, are presented and their advantages and drawbacks are compared. IR-UWB is employed in this thesis due to its relatively simple receiver architecture. The principle of Rake receivers for wireless applications is also discussed in this chapter. ARake, SRake and PRake are described and compared. The major drawback associated with conventional Rake structure is that it requires channel information including multipath delays and attenuations to be known or correctly estimated at the receiver end, which is not practical in real life UWB applications.

The BRake receiver architecture is presented in chapter 3. Firstly system model is discussed. BPSK modulation is employed in our system to simplify the following mathematical analysis. Multipath channel models CM1-CM4 for UWB indoor channels are adopted. BRake receiver structure is then proposed with the branch and tap number determination criterion.

Chapter 4 focuses on performance analysis. It begins with correlation receiver since Rake

structures are basically a combination of correlation receivers. MMSE criterion is used to determine the optimum tap weights and Wiener solution is obtained. LMS method is employed during adaptation phase, and there is an error term associated with the adaptation step size. This is also discussed in this chapter. Output SNR is then calculated and closed form BER is obtained based on it.

Extensive simulations are carried out and the significant results are given in chapter 5. Theoretical analysis is proved to be valid by comparing with the simulated BER. There is a complicated term associated with step size which is ignored previously to simplify the SNR expression. To verify the appropriateness of dropping this term, the effect of the step size on the approximation is examined. Finally, the performance of the proposed structure is also compared with ARake and SRake. It is proved that the proposed structure requires no channel state information and achieves a much reduced sampling rate with insignificant performance loss comparing with conventionally Rake receivers.

6.2 Future Works

The parameter η, which represents the successfully collected channel energy, is determined by the distribution of the tap weights in this thesis. The channel models can be further studied and there may exist some relationships between channel models parameters, branch numbers, tap numbers, sampling rates, and η. If this is the case, then η could be optimistically obtained by choosing proper system parameters to boost the system performance.

The algorithm for the BRake receiver has been designed. However the simulation is carried out in system level not circuit level. The next step is to do the hardware implementation, with the ultimate goal to integrate the whole system to a Field Programmable Gate Array (FPGA) or Application-Specific Integrated Circuit (ASIC).

REFERENCES

[1] T. W. Barrett, "History of ultra wideband (UWB) radar and communications: Pioneers and innovators," in *Proc. Progress in Electromagnetics Symposium*, Cambridge, MA, 2000.

[2] G. F. Ross, "The transient analysis of multiple beam feed networks for array systems," *Ph.D. dissertation*, Polytechnic Institute of Brooklyn, Brooklyn, NY, 1963.

[3] G. F. Ross and K. W. Robbins, *Base-band radiation and reception systems*, U.S. Patent 3,739,392, June 12, 1973.

[4] J. D. Taylor, *Introduction to Ultra Wideband Radar Systems*. Boca Raton, FL: CRC, 1995.

[5] http://www.multispectral.com

[6] R. A. Scholtz, "Multiple access with time-hopping impluse modulation," presentd at the Conf. Milcom, Bedford, MA, 1993.

[7] M. Z. Win and R. A. Scholtz, "Ultra-wide bandwidth time hopping spread-spectrum impulse radio for wireless multiple access communications," *IEEE Trans. Commun.*, vol. 48, pp. 679-690, Apr. 2000.

[8] M. Z. Win and R. A. Scholtz, "Impulse radio: How it works," *IEEE Commun. Lett.*, vol. 2, pp. 36-38, Feb. 1998.

[9] M. Z. Win and R. A. Scholtz, "On the robustness of ultra-wide bandwidth signals in dense multipath environments," *IEEE Commun. Lett.*, vol. 2, pp. 51-53, Feb, 1998.

[10] FCC First Report and Order: In the matter of Revision of Part 15 of the Communication's Rules Regarding Ultra-Wideband Transmission Systems, *FCC 02-48*, April 2002.

[11] A. Batra, J. Balakrishnan, G. R. Aiello, J. R. Foerster and A. Dabak, "Design of a multiband OFDM system for realistic UWB channel environments," *IEEE Trans. Microwave Theory and Techniques*, vol. 52, No. 9, September 2004.

[12] C. E. Shannon, *The Mathematical Theory of Information*. Urbana, IL:University of Illinois Press, 1949.

[13] M. Z. Win and R. A. Scholtz, "Characterization of ultra-wide bandwidth wireless indoor channels: a communication-theoretic view," *IEEE Journal on Selected Areas in Communications,* vol. 20, No. 9, Dec. 2002.

[14] IEEE P802.15-02/368r5-SG3a.

[15] A. A. Saleh and R. Valenzuela, "A statistical model for indoor multipath propagation," *IEEE J. Select. Areas Commun*., vol 5, pp. 128-137, Feb. 1987.

[16] G. R. Aiello and G. D. Rogerson, "Ultra-wideband wireless systems," *IEEE Microwave Mag.*, vol. 4, No. 2, pp. 36-47, 2003.

[17] J. Balakrishnan, A. Batra, and A. Dabak, "A multi-band OFDM system for UWB communication," in *Proc. Conf. Ultra-Wideband Systems and Technologies, Reston*, VA, 2003, pp. 354-358.

[18] E. Saberinia and A. H. Tewfik, "Pulsed and non-pulsed OFDM ultra wideband wireless personal area networks," in *Proc. Conf. Ultra-Wideband Systems and Technologies, Reston*, VA, 2003, pp 275-279.

[19] A. Batra, J. Balakrishnan, and A. Dabak, "Multi-Band OFDM: a new approach for UWB," *IEEE ISCAS*, vol. 5, V-365 – V-368, May 2004.

[20] S. Roy, J. R. Foerster, V. S. Somayazulu, and D. G. Leeper, "Ultrawideband radio design: the promise of high-speed, short-range wireless connectivity", *IEEE Proceddings*, vol. 92, No. 2, Feb. 2004.

[21] R. Kolic, "Ultra wideband- the next-generation wireless connection," http://www.deviceforge.com/articles/AT8171287040.html.

[22] L.Q. Yang and G. B. Giannakis, "Ultra-wideband communication: an idea whose time has come," *IEEE Signal Processing Magazine*, vol. 21, Issue 6, pp. 26 – pp. 54, Nov. 2004.

[23] H. Sheng, P. Orlik, A. M. Haimovich, L. J. Cimini and J. Zhang, "On the spectral and power requirements for ultra-wideband transmission." *IEEE International Conference on Communications*, vol. 1, pp 11-15, May 2003.

[24] L. E. Miller, "Autocorrelation functions for Hermite-polynomial ultra-wideband pulses," *IEE Electronics Letters*, vol. 39, No. 11, May 2003.

[25] Y. Wu, A. F. Molisch, S. Y. Kung and J. Zhang, "Impulse radio pulse shaping for ultra-wide bandwidth (UWB) systems," *IEEE International Symposium on Personal, Indoor and Mobile Radio Communication Proceeding*, 20003.

[26] L. E. Miller, "Models of UWB pulses", *NIST*, May 2003.

[27] L. Zhao and A. M. Haimovich, "Performance of ultra-wideband communications in the presence of interference," *IEEE J. Select. Areas Commun.*, vol. 20, No. 9, Dec 2002.

[28] C. C. Chui and R. A. Scholtz, "Optimizing tracking loop for UWB monocycles," in *Proc. IEEE Global Telecommunications Conference*, vol. 1, pp. 425-430, Dec. 2003.

[29] F. R. Mireles and R. A. Scholtz, "N-orthogonal time-shift-modulated signals for ultra wide bandwidth impulse radio modulation," in *Proc. IEEE Mini Conf. Communication Theory,* Phoenix, AZ, 1997, pp. 245-250.

[30] H. Liu, "Error performance of a pulse amplitude and position modulated ultra-wideband system over lognormal fading channels," *IEEE Communication Letters*, vol. 7, No. 11, Nov. 2003.

[31] J. G. Proakis, *Digital Communication*, 4th edition, New York: McGraw-Hill, 2001.

[32] M. Z. Win and R. A. Scholtz, "On the energy capture of ultra-wide bandwidth signals in dense multipath enviroments," *IEEE Commun. Lett*., vol. 2, pp. 245-247, Sept. 1998.

[33] M. Z. Win and Z. A. Kostic, "Virtual path analysis of selective Rake receiver in dense multipath channels," *IEEE Commun. Lett*., vol. 3, pp. 308-310, Nov. 1999.

[34] M. Z. Win, G, Chrisikos, and N. R. Sollenberger, "Performance of Rake reception in dense multipath channels: implications of spreading bandwidth and selection diversity order," *IEEE J. Select. Areas Commun*., vol. 18, pp. 1516-1525, Aug. 2000.

[35] M. Z. Win and G. Chrisikos, "Impact of spreading bandwidth and selection diversity order on selective Rake reception," in *Wideband Wireless digital communications* (A. F. Molisch, ed.), pp. 424-454, Prentice Hall Publishers, 2001.

[36] D. Cassioli, M. Z. Win, F. Vatalaro and A. F. Molisch, "Performance of low complexity Rake reception in a realistic UWB channel," *IEEE International Conference on Communications*, vol. 2, pp. 763-767, May 2002.

[37] W. Q. Malik, D. J. Edwards and C. J. Stevens, "Experimental evaluation of Rake receiver performance in a line-of-sight ultra-wideband channel," *International Workshop on Joint UWBST & IWUWBS*, pp. 217-220, May 2004.

[38] M. A. Rahman, S. Sasaki, J. Zhou, S. Muramatsu, and H. Kikuchi, "Evaluation of selective Rake receiver in direct sequence ultra wideband communications in the presence of interference," *International Workshop on Joint UWBST & IWUWBS*, pp. 221-225, May 2004.

[39] M. Eslami and X. Dong, "Performance of Rake-MMSE-Equalizer for UWB communications," *IEEE Wireless Communication and Networking Conference*, vol. 2, pp. 855-860, Mar. 2005.

[40] A. Rajeswaran, V. S. Somayazulu, and J. R. Foerster, "Rake performance for a pulse based UWB system in a realistic UWB indoor channel," *IEEE International Conference on Communications*, vol. 4, pp. 2879-2883, May 2003.

[41] M. Eslami and X. Dong, "*Rake-MMSE-Equalizer performance for UWB," IEEE Communications Letters*, vol. 9, No. 6, June 2005.

[42] B. Mielczarek, M. O. Wessman and A. Svensson, "Performance of coherent UWB Rake receivers with channel estimators," *IEEE Vehicular Technology Conference*, vol. 3, pp. 1880-1884, Oct. 2003.

[43] H. Sheng, A. M. Haimovich, A. F. Molisch and J. Zhang, "Optimum combining for time hopping impulse radio UWB Rake receivers," *IEEE Conference on Ultra Wideband Systems and Technologies*, pp. 224-228, Nov. 2003.

[44] H. Niu, J. A. Ritcey and H. Liu, "Performance of UWB Rake receivers with imperfect tap weights," *in Proc. IEEE International Conference on Acoustics, Speech and Signal Processing*, 2003.

[45] F. E. Aranda, N. Brown, and H. Arslan, "Rake receiver finger assignment for ultra-wideband radio," *IEEE Workshop on Signal Processing Advances in Wirelsess Communications*, 2003.

[46] S. Gezici, M. Chiang, H. V. Poor and H. Kobayashi, "Optimal and suboptimal finger selection algorithms for MMSE Rake receivers in impulse radio ultra-wideband systems," *IEEE Wireless Communication and Networking Conference*, vol. 2, pp. 861-866, Mar. 2005.

[47] V. Lottici, A. D. Andrea, and U. Mengali, "Channel estimation for ultra-wideband communications,", *IEEE. J. Select. Areas Commun.*, vol. 20, no. 9, pp. 1638-1645, 2002.

[48] C. Carbonelli, U. Mengali, and U. Mitra, "Synchronization and channel estimation for UWB signals," in *Proc. Global Telecommunications conf.*, San Franscisco, CA, 2003, pp. 764-768.

[49] C. Carbonelli and U. Mitra, "Clustered channel estimation for UWB signals," *IEEE International Conference on Communications*, vol. 4, pp. 2432-2436, June 2004.

[50] S. S. Tan, A. Nallanathan, B. Kannan, "A pilot symbol assisted channel estimation scheme for UWB IR systems with diversity reception," *IEEE Eighth International Symposium on Spread Spectrum Techniques and Applications*, pp. 483-487, Sept. 2004.

[51] B.B. Farhang, *Adaptive Filers Theory and Applications*, John Wiley & Sons, West Sussex, UK 1998.

[52] J. Sherman and W. J. Morrison, "Adjustment of an inverse matrix corresponding to a change in one element of a given matrix," *Ann. Math. Statist.,* vol. 21, pp. 124-127, 1950

[53] S. Haykin, *Adaptive Filter Theory*, 4th Edition, Prentice Hall, NJ, USA 2002

LIST OF PUBLICATIONS

[1] Y. J. Zheng, M. Z. Cao, L. Yang, and H. K. Garg, "An Adaptive Filtering System for Direct Conversion Receivers: Architecture and Performance Analysis," submitted to *IEEE Transactions on Circuits and Systems I*, Jan. 2006.

[2] Y. J. Zheng, J. H. Ng, and L. Yang, "A Low-Complexity Blind Rake Combining Equalizer for UWB Communication Systems," accepted by *International Conference on Ultra Wideband,* Sept. 2006.